https://doi.org/10.5194/essd-2026-623
Preprint. Discussion started: 21 August 2026

The Hyperspectral Bio-Optical Observations Sailing on Tara (HyperBOOST) dataset

Margherita Costanzo[1,2], Vittorio Ernesto Brando[1], Federico Falcini[1], Christian Marchese[1], Luis Gonzalez Vilas[1,3], Emmanuel Boss[1,4], David Doxaran[5], Paola Potin[5], Stefan Simis[6], Tom Jordan[6], John Wood[7], Chiara Santinelli[8], Giancarlo Bachi[8], Giovanni Checcucci[8], Claudia Tropea[8], Marco Carloni[8], Mirco Guerrazzi[8], Silvia Valsecchi[8], Valtere Evangelista[8], Marie Helene Rio[9], Javier Alonso Concha[9,10], Paola Bertucci[11], Colomban de Vargas[12], Victor Martinez-Vicente[6], Tara Europa Team[13], TREC-Tara Europa Operation and Management Team[13], TREC Consortium Coordinators[13]

[1]Consiglio Nazionale delle Ricerche (CNR), Istituto di Scienze Marine (ISMAR), 00133 Rome, Italy
[2]Dipartimento Ingegneria civile, edile e ambientale, Università Sapienza, Rome, Italy
[3]Nologin Oceanic Weather Systems, 15705 Santiago de Compostela, Spain
[4]School of Marine Sciences, University of Maine, Orono, Maine
[5]Laboratoire d'Océanographie de Villefranche, UMR 7093, CNRS / Sorbonne Université, Villefranche-Sur-Mer, France
[6]Plymouth Marine Laboratory, PL13DH Plymouth, United Kingdom
[7]Peak Design Ltd, DE4 2DH Winster, United Kingdom
[8]Consiglio Nazionale delle Ricerche (CNR), Istituto di Biofisica (IBF), Pisa, Italy
[9]European Space Agency, 00044 Frascati, Italy
[10]Serco Italia S.p.A. for ESA, 00173 Rome, Italy
[11]European Molecular Biology Laboratory, 69117 Heidelberg, Germany
[12]CNRS/Sorbonne University, Station Biologique de Roscoff, Roscoff, France
[13]A full list of authors appears at the end of the paper

Correspondence: Vittorio Ernesto Brando (vittorio.brando@cnr,it)

Abstract. During the Tara Europa Expedition, the HyperBOOST (Hyperspectral Bio-Optical Observations Sailing on Tara) team, part of the larger research program TREC (TRaversing European Coastlines), carried out the collection of discrete and continuous measurements to explore the bio-optical properties of water at the land-sea interface. During the 409 days of the expedition between April 2023 and August 2024, 202 HyperBOOST stations were sampled along the European coastlines, including the Baltic Sea, the North Sea and the Mediterranean Sea. Discrete biogeochemical samples were collected in triplicate at all stations using Niskin bottles, including dissolved and particulate organic carbon, suspended particulate matter, chlorophyll *a* and other biologically relevant pigments, as well as samples for dissolved and particulate absorption. Along-track continuous AOP measurements were carried out using a So-Rad (solar tracking radiometry platform), while IOPs were collected and processed through the automated In-line system/software. After binning and quality control, 236,567 one-minute binned particulate absorption and attenuation spectra, 26,589 five-minute binned back-scattering spectra, and 7001 five-minute binned So-Rad reflectance spectra were available for further analyses and colocation with the station data. Overall, the Tara Europa expedition allowed to

https://doi.org/10.5194/essd-2026-623
Preprint. Discussion started: 21 August 2026

systematically sample European coastal waters at unprecedented temporal and spatial coverage, crossing regions characterized by a wide range of optical and biogeochemical conditions. The combined use of different instruments or measurements approaches also provided the opportunity to assess the internal consistency of the dataset by performing several optical closure assessments. The HyperBOOST dataset provides a valuable resource for advancing and evaluating existing and devising novel bio-optical models in optically diverse waters, enhancing satellite ocean-colour applications and product validation.

1 Introduction

A key requirement for validating satellite-derived ocean products is the temporal and spatial overlap between in situ and satellite observations, which is essential for accurately quantifying the performance and limitations of these data streams. The development and refinement of ocean-colour algorithms similarly rely on high-quality *in situ* measurements, both as independent references and in combination with satellite observations. Notably, since the pioneering COASTℓOOC program introduced by Babin et al. (2003), no coordinated initiative has systematically measured optical properties across the full extent of the European coastal domain. Although logistically demanding and costly, oceanographic cruises remain an essential means of collecting and analysing biogeochemical and optical data and are indispensable for both research and long-term monitoring of marine ecosystems. In this context, the Tara Europa Expedition provided a unique opportunity to address this gap, and to enable the deployment of novel optical sensors.

Specifically, the Tara Europa Expedition was conducted in 2023 and 2024 as part of the Traversing European Coastlines Project (TREC), led by the European Molecular Biology Laboratory (EMBL). A defining feature of the Tara Europa-TREC campaign was the coordinated sampling of terrestrial and marine stations designed to investigate land–ocean connectivity. To this end, the project integrated ocean exploration with parallel sampling of soils, sediments, shallow waters, and selected model organisms across a broad range of terrestrial and aquatic habitats, and several imaging and -omics measurements were collected though discrete sampling or using the Tara the in-line system (De Vargas et al., 2015; Sunagawa et al., 2015, 2020). This integrated approach enabled the systematic characterization of environmental and biogeochemical gradients along European coastlines.

The Tara Europa-TREC expedition was conducted between April 2023 and July 2024. During this period, researchers aboard the schooner Tara sampled 188 coastal stations. Within this framework, the Hyperspectral Bio-Optical Observations Sailing on Tara (HyperBOOST) project expanded the *in-situ* sampling to include a comprehensive suite of bio-optical and biogeochemical measurements relevant to current and forthcoming satellite ocean-colour missions (e.g., NASA PACE, Copernicus Flex and CHIME). This sampling effort provided broad spatial coverage across diverse coastal environments, as well as targeted observations in offshore blue waters on 14 stations in August 2024, thereby strengthening the representativeness of the dataset. This paper describes the data collected during the 2023-2024 period as part of the HyperBOOST research project conducted aboard the schooner Tara. Measurements were acquired both at discrete stations and continuously.

https://doi.org/10.5194/essd-2026-623
Preprint. Discussion started: 21 August 2026

Open Access Earth System Science Data Discussions

Consistent with previous Tara expeditions (e.g., (Boss et al., 2013; Chase et al., 2017; Sunagawa et al., 2020; Werdell et al., 2013a), inherent optical properties (IOPs) were obtained using the in-line system and associated software, while discrete biogeochemical samples, including dissolved organic carbon (DOC), total organic carbon (TOC), suspended particulate matter (SPM), and chlorophyll *a* (Chla), were collected at all stations using Niskin bottles, and hyperspectral remote-sensing reflectance (R_{rs}) was measured at selected stations with a Hyperspectral Tethered Spectral Radiometer Buoy (HTSRB) system. Aiming to meet the *in situ* observation requirements for planktonic ecosystems and for aquatic carbon studies detailed in Dierssen et al., (2020) and Lombard et al. (2019), additional samples for particulate absorption were collected at all stations using Niskin bottles, and hyperspectral above-water R_{rs} was measured continuously using the Solar-tracking radiometry platform (So-Rad) (Jordan et al., 2022; Wright and Simis, 2021).

Owing to its extensive temporal and spatial coverage, the HyperBOOST dataset provides a valuable resource for advancing and evaluating novel bio-optical models in optically diverse waters.

Accordingly, the primary aim of this paper is to describe the HyperBOOST dataset that is relevant for satellite ocean-colour applications.

2 Study area and measurement overview

2.1.1 Sampling strategy

Overall, 202 stations were sampled aboard Tara during the 2023-2024, spanning 21 European countries (Figure 1). Sampling was conducted from 30 March to 9 November 2023 along the coasts of the Baltic Sea, North Sea, and Atlantic Ocean; from 29 February to 30 July 2024 along the Mediterranean Sea coasts; and in Mediterranean Sea open blue-water environments from 31 July to 22 August 2024. In addition to discrete station sampling, optical measurements were continuously acquired along the ship's track.

The Tara Europa in situ sampling strategy was designed to complement the TREC land transects, which focused on soils, intertidal zones, and shallow coastal waters. To ensure consistency across the land–sea continuum, marine stations were systematically chosen within the coastal biogeochemical domain in proximity to the corresponding shoreline sites sampled by the EMBL land teams. These marine stations were usually placed about 1 km offshore at depths of roughly 15 m, allowing safe deployment of oceanographic equipment while still representing nearshore biogeochemical conditions. Additional stations were set up in estuaries and similar transitional environments to create inshore-offshore transects, enabling the sampling of biogeochemical and optical property gradients across coastal systems (Marchese et al., 2024). Station selection was based on high-resolution Chla climatology derived from multi-year regional satellite products (Brando et al., 2024), providing information on the most probable spatial patterns and fine-scale coastal variability at each target site. Interactive Leaflet-based maps were used to facilitate data sharing and real-time visualization among the Tara Europa sampling strategy team and the scientific crew aboard Tara (Marchese et al., 2024). When available under cloud-free conditions, near-real-time satellite imagery of Chla and suspended particulate matter (SPM) was also used as situational "snapshots" to identify departures from climatological conditions or

https://doi.org/10.5194/essd-2026-623
Preprint. Discussion started: 21 August 2026

to detect transient features such as fronts, eddies, or upwelling events. In such cases, updated Leaflet maps displaying near-real-time data and proposed station locations were shared with the scientific crew aboard Tara, enabling adaptive refinement of sampling plans in response to evolving oceanographic conditions (Marchese et al., 2024).

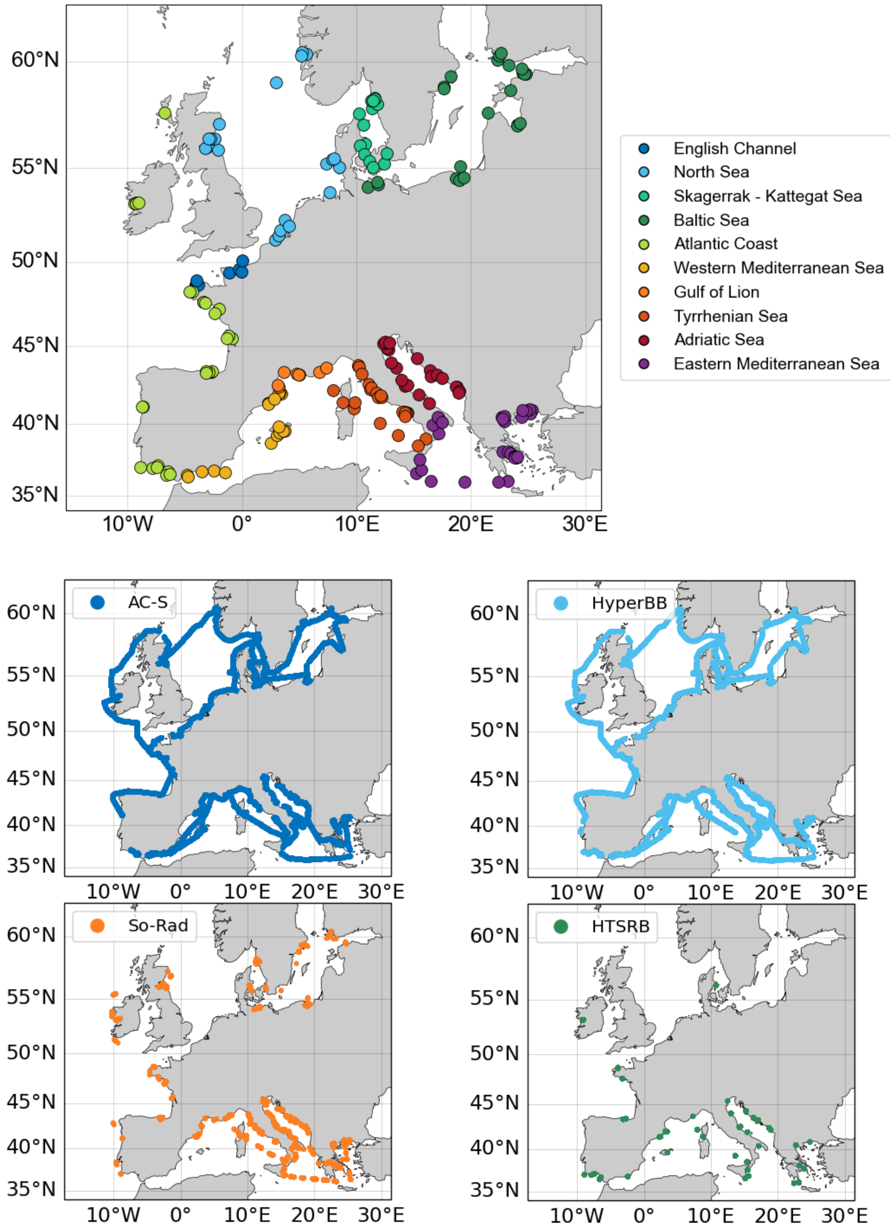

Figure 1. Map of the sampling stations of the Tara Europa Expedition. Ninety-nine stations were sampled during 2023, from April to November. In 2024, eighty-nine stations were sampled along the

https://doi.org/10.5194/essd-2026-623
Preprint. Discussion started: 21 August 2026

Open Access Earth System Science Data Discussions

Mediterranean coasts. Finally, the HyperBOOST leg in August 2024 covered blue waters by sampling fourteen stations. The top panel reports the sampling stations of the Tara Europa Expedition for 2023 and 2024 and the HyperBOOST leg, colour coded by regions. Then the four smaller panels provide the spatial coverage of data collected continuously with the In-line system for IOPs (ACS and HyperBB) and using the So-Rad and HTSRB for R_{rs}.

3 Measurements methods and data reduction

3.1 Measurement overview

The HyperBOOST dataset encompasses *in situ* data collected at discrete stations and continuously, as well as laboratory measurements performed on discrete samples collected in the field (Table 1). At all the 202 stations (Figure 1), discrete samples were collected in triplicate from Niskin bottles deployed on the rosette, which also hosted a conductivity-temperature-depth (CTD) profiler (Seabird SBE911). All sampling protocols were provided to the Tara sampling team and water was filtered on board accordingly (Guillam et al., 2026). Water samples for DOM analyses were shipped to the lab within two weeks, while all filters were shipped to EMBL in Heidelberg (Germany) at every major stop and, where they were stored and then sent to LOV only at the end of each year. Several of the parameters reported in Table 1 have been collected in previous TARA expeditions (Boss et al., 2013; Chase et al., 2017; Sunagawa et al., 2020; Werdell et al., 2013b); new observations collected for the first time in TARA, within the ESA HyperBOOST project included the discrete samples for particulate absorption (a_p), suspended particulate matter (SPM) and particulate organic carbon (POC) , inline hyperspectral back scattering (b_{bp}) with the HyperBB and automated above-water radiometry using the So-Rad (Jordan et al., 2022; Wright and Simis, 2021) and HSR-1 (Hyperspectral radiometer) (Wood et al., 2017).

This section provides an overview of the methods for laboratory measurements on discrete samples and continuous measurements.

Table 1 Summary of variables collected during Tara Europa. (d) derived

Data category	Quantity	Acronym / Symbol	Units	Instrument
AOP	Remote-sensing reflectance	R_{rs}	sr^{-1}	So-Rad and HTSRB
	Normalized water-leaving radiance	L_{wn}	µW cm^{-2} sr^{-1}	So-Rad and HTSRB
	Spectral Downwelling Irradiance	E_d	µW cm^{-2} nm^{-1}	So-Rad, HTSRB, HSR-1

https://doi.org/10.5194/essd-2026-623
Preprint. Discussion started: 21 August 2026

	Spectral Downwelling Diffuse and Direct Irradiance	E_{ds} E_{dd}	µW cm^{-2} nm^{-1}	HSR-1
IOP	CDOM absorption coefficient	a_{CDOM}	m^{-1}	samples
	Phytoplankton absorption coefficient	a_{phy}	m^{-1}	samples
	Particulate absorption coefficient	a_p	m^{-1}	samples
	Non-algal particles absorption coefficient	a_{NAP}	m^{-1}	samples
	Non-water absorption coefficient	a_{nw}	m^{-1}	Samples (d)
	Particulate absorption coefficient	a_p	m^{-1}	AC-S
	Particulate scatter coefficient	c_p	m^{-1}	AC-S
	Particulate backscatter coefficient	b_{bp}	m^{-1}	HyperBB
	Phytoplankton absorption coefficient	a_{phy}	m^{-1}	AC-S (d)
	CDOM absorption coefficient	a_{CDOM}	m^{-1}	FDOM (d)
	Non-algal particles absorption coefficient	a_{NAP}	m^{-1}	AC-S (d)
	Non-water absorption coefficient	a_{nw}	m^{-1}	AC-S (d)
BGC	Total chlorophyll-a concentration	*TChla*	mg m^{-3}	HPLC
	Phytoplankton pigments concentration		mg m^{-3}	HPLC
	Total suspended matter concentration	*SPM*	mg L^{-1}	gravimetry
	Particulate Inorganic Fraction	*PIF*	%	gravimetry
	Particulate Organic Fraction	*POF*	%	gravimetry
	Fluorescence Chlorophyll	*FChl*	RFU	
	Dissolved Organic Fluorescence	*FDOM*	RFU	Seapoint sensor
	Dissolved Organic Carbon concentration	*DOC*	µM	Discrete samples
	Total Organic Carbon concentration	*TOC*	µM	Samples and (d)

https://doi.org/10.5194/essd-2026-623
Preprint. Discussion started: 21 August 2026

	Particulate Organic Carbon concentration	*POC*	µM	samples
	Total chlorophyll-a derived from AC-S	*TChla(AC-S)*	mg m^{-3}	AC-S (d)
	Turbidity	*Turb*	FNU	samples

3.2 Laboratory measurements on discrete samples

3.2.1 Dissolved organic matter

All the samples for dissolved organic carbon (DOC), and chromophoric dissolved organic matter (CDOM) were filtered directly from the Niskin bottles, using a portable filtration device implemented at CNR-IBF and a 0.2 mm Sterivex filter (SVGV010RS), washed with 200 ml of MilliQ water. Unfiltered samples were also collected for the analyses of total organic carbon (*TOC*). Samples for DOC and TOC were immediately acidified to pH < 2 using ultrapure 2M HCl. All the samples were immediately stored on board in the dark and at 4°C and analysed within 2 weeks from the sampling to minimise problems associated with the long storage.
DOC and TOC measurements were carried out with a Total Organic Carbon analyzer (TOC-L, Shimadzu), by high temperature catalytic oxidation, following (Santinelli et al., 2015). Measurement quality was assessed twice daily by comparison of data with DOC Consensus Reference Materials (CRM batch *#23/02*, measured concentration: 41.4 ± 1.6 µM, n =55) (Hansell, 2005).
CDOM absorbance spectra (a_{CDOM}) were measured throughout the UV and visible spectral domains (230–700 nm) using a UV-visible spectrophotometer (Shimadzu, uv-2600i), with a 10 cm quartz cell, following (Galletti et al., 2019). Milli-Q water is used as a reference, and its spectrum is subtracted from each sample. The absorbance data were converted into an absorption coefficient by using Eq. (1):

$$\boldsymbol{a}_{l} = \boldsymbol{A}_{l}\,\frac{\mathbf{2.303}}{\mathbf{L}} \tag{1}$$

where A_λ is the absorbance at the wavelength λ and L is the cuvette pathlength expressed in m.

3.2.2 Water turbidity, suspended particulate matter, particulate organic and inorganic carbon

Samples for turbity (TU) and suspended particulate matter (SPM) were transferred directly from the Niskin to a Nalgene container, which was regularly gently mixed to maintain a homogeneous concentration of suspended particles. Following the protocol defined by Dogliotti et al. (2015), the water turbidity (in Formazine nephelometric unit (FNU)) was measured in triplicate on Tara. The mean turbidity value measured was used to determine the optimal volume of water sample to be filtered (in triplicate) through pre-combusted and pre-weighed glass-fibre filters (Whatman GF/F, 25 mm) (Neukermans et al., 2012). These filters were rinsed with Milli-Q water, then immediately stored at -

https://doi.org/10.5194/essd-2026-623
Preprint. Discussion started: 21 August 2026

80°C, and shipped to the laboratory at the end of each campaign. They were dried and reweighed in the laboratory first for PM determination (in g·m^{-3}), then for measuring POC content and associated stable isotopes (Blasco et al., 2021). Based on the triplicates throughout the expedition, the mean propagated standard deviation associated with SPM measurements was 0.29 g m^{-3}, resulting in a mean relative uncertainty averaged across the dataset of 13.9%.
Another set of pre-combusted and pre-weighed glass-fibre filters (Whatman GF/F, 25 mm) was used to filter (in triplicate) the same volume of water for subsequent determination of the particulate organic and inorganic mass fractions (POF and PIF in %) by ashing (4 h at 450°C), then reweighing of filters(IOCCG, 2021). It should be noted that in some cases, the total mass of particles retained on filters disappeared, i.e., we retrieved the initial mass of dry filters before filtration of water samples. In these cases, we assumed that particles were 100% organic, i.e., POF = 100% and PIF = 0%.

3.2.3 Light absorption coefficient (PA) of suspended particles

The same volume (or up to 20% less if the water was highly turbid) of the water sample was filtered through new GF/F filters in subdued light, with the regular face of the GF/F filter up on the filter holder. The filter was rinsed with 250 ml of pure (milli-Q) water, removed from the filter holder, and put on a circular petri-dish, which was stored at -80°C until laboratory analyses. The light absorption coefficients of total, non-algal, and by difference of algal particles (a_p, a_{NAP} and a_{phy}, in m^{-1}) were measured using a Perkin-Elmer Lambda 650 UV/Vis Spectrophotometer equipped with a 150 mm Spectralon integrating sphere. Filters were taken out from the freezer one by one and left for a few minutes at ambient temperature, under subdued light conditions, then placed in the centre of the integrating sphere using a specifically designed filter holder. Light absorbance or optical density (OD) was measured from 350 to 800 nm with a spectral resolution of 1 nm. The absorption coefficients (in m^{-1}) were computed from the measured OD (*ODsample)* values as (IOCCG protocol, 2021):

$$a(\lambda) = \ln(10)\ \mathrm{ODs}(\lambda)/L \quad \textbf{(2)}$$

With the optical pathlength L = V/A, the volume of water sample filtered and A the filter clearance. The optical density of a blank filter (*ODblank*) saturated with pure water was measured every 6 sample filters analysed, before and after staying 1 h in methanol, so that the absorption coefficient of total particles (a_p) was computed as:

$$\mathrm{ODf} = \mathrm{ODsample} - \mathrm{Odblank} \quad \textbf{(3)}$$

$$a_p(\lambda) = \ln(10)\ (\mathrm{ODf} - \mathrm{ODblank})(\lambda)/L \quad \textbf{(4)}$$

Finaly a correction was applied to take into account amplification of the optical pathlength within the filter, according to:

Integrating sphere (IS) mode: ODs = 0.323 (ODf)1.0867 **(5)**

https://doi.org/10.5194/essd-2026-623
Preprint. Discussion started: 21 August 2026

The filter was placed back on the filter holder, face up, for one hour with the filtration funnel filled with 100 ml of methanol for the removal of phytoplankton pigments. The methanol with dissolved phytoplankton pigments was aspirated through a filter, which was then re-saturated with pure water and placed back in the centre of the integration sphere to measure light absorption by non-algal particles (a_{NAP}). The light absorption coefficient of algal particles was then determined as:

$$a_{phy}(\lambda) = a_p(\lambda) - a_{NAP}(\lambda) \quad \textbf{(6)}$$

Significant a_{phy} residual values obtained from 700 to 750 nm were assumed to be measurement errors, and the offset estimated as the average a_{phy}(700-750 nm) value was subtracted from the whole a_{phy} spectrum (Babin et al., 2003b; Babin and Stramski, 2004).

3.2.4 HPLC analyses for phytoplankton pigments determination

For phytoplankton pigments determination, the same volumes of water samples as for TU and SPM were filtered through 25 mm Whatman GF/F filters that were placed in vials, immediately frozen in liquid nitrogen then stored at -20°C onboard and -80°C on land until laboratory analyses at LOV. The determination and quantification of up to thirty pigments, when present, was carried out by the SAPIGH, the French National Analytical Service dedicated to HPLC (High-Performance Liquid Chromatography) following the protocol defined by (Ras et al., 2008).
In this work the total chlorophyll-a (TChla, mg.m^{-3}) concentration was defined as the sum of chlorophyll-a (chla), divinyl chlorophyll-a (DVchla) and chlorophyllide-a (chld-a). Throughout the expedition, triplicate measurements of TChla were performed at 15 stations: the resulting mean standard deviation associated with TChla measurements was 0.12 mg.m^{-3}, resulting in a mean relative uncertainty of 4.67%.

3.3 Continuous measurements

3.3.1 IOP inline system

In-line optical system instruments (AC-S, HyperBB, Seapoint UV fluorometer) were recorded on Tara using the Inlinino software datalogger(Haëntjens, 2026; Haëntjens and Boss, 2020) and were processed using the Inline-Analysis software package (https://github.com/OceanOptics/InLineAnalysis). In addition, a thermo-salinograph (SBE 45) was installed, providing temperature and salinity data. All in-line instruments were logged on the same computer which was synchronized with the ship's GPS date/time and latitude/longitude over the NMEA.
The dissolved organic fluorescence (FDOM) was collected with a Seapoint UV fluorometer (ex 370 em 440) within the in-line system in units of volts. The data showed a significant correlation with the CDOM and DOC discrete samples, allowing for an interpolation of DOC and CDOM between stations. It was also used in the correction of the AC-S and HyperBB data, so that high frequency changes in IOPs between filtered events could be accounted for.

https://doi.org/10.5194/essd-2026-623
Preprint. Discussion started: 21 August 2026

Hyperspectral absorption and attenuation were measured continuously on board the R/V Tara during the Tara Europa Expedition using a WetLabs AC-S spectrophotometer. The AC spectrophotometer was set after a switching system running 0.2 um filtered seawater through the instrument for the first 10 minutes of every hour, and total (“normal”) seawater was flowing the rest of the time. This setup allows for the retrieve of particulate absorption (a_p) and attenuation (c_p) independently from the instrument drift and the biofouling effect (Dall’Olmo et al., 2009; Slade et al., 2010). Every 5-7 days the AC-S and FDOM sensors were cleaned and the filter was changed.

AC-S data was processed following Boss et al. (2019) as modified in Bourdin et al. (2026), using a custom software for in-line optical data processing (https://github.com/OceanOptics/InLineAnalysis/). Total and filtered data were first separated according to flow data of the in-line data. The processing followed the description on Bourdin et al., 2026, and is briefly described below.

Particulate spectra were computed as the difference between total and interpolated dissolved spectra from the periods before and after the ‘total’ measurement periods using the FDOM fluorometer. All a_p and c_p spectra were unsmoothed following the method in Chase et al. (2013). Additionally, temperature and salinity corrections were carried out based the AC-S specific temperature and salinity tables of (Sullivan et al., 2006). Finally, all spectra were inspected by a trained operator and unreasonable spectra were removed. This resulted in a total of 236,567 a_p and c_p binned spectra available for further analysis.

The scattering correction applied is based on a blend of the proportional correction method (Zaneveld et al., 1994) and an offset in red inspired from (Röttgers et al., 2013), and was found to perform best when compared with discrete measurements collected throughout the Tara Europa two-year expedition:

$$a_{p,corr}(\lambda) = a_{p,Tcorr}(\lambda) - \frac{c_{p,Tcorr}(715)}{c_{p,Tcorr}(715)} c_{p,Tcorr}(\lambda) + 0.0854 a_{ac-s,m}. \quad \textbf{(7)}$$

Where T_{corr}- corrected for temperature changes relative to factory calibration.

The hyper-spectral backscattering coefficient $bb_p(\lambda)$ was derived from continuous measurements of Volume scattering function (VSF) acquired using a HyperBB (Sequoia Sci.) set in 2L specially constructed container. The VSF $\beta_{measured}(\theta_0, \lambda)$ measuremetes near 135° from 430 to 700 nm at 10 nm resolution were acquired using the same switching system as the AC=S, running 0.2 um filtered sea water through the box during the first 10 minutes of every hour, and total (non-filtered) seawater the rest of the hour. This setup allows to retrieve particulate VSF (β_p) independently from instrument drift, box effect, biofouling, and particle accumulation happening in the box.

The details on the derivation of the particulate VSF ($\beta_p(\theta_0, \lambda)$) from $\beta_{measured}(\theta_0, \lambda)$ are provided in Zhou et al. (2026) and in Boss et al. (2026). Then, the hyper-spectral particulate backscattering coefficient $bb_p(\lambda)$ can be retrieved as:

$$bb_p(\lambda)=2*\pi*\chi(135°)*\beta_p(135°,\lambda). \quad \textbf{(8)}$$

where $\chi(135°) = 1.177$ is the weighted mean of the data in table 6.1 in (Sullivan et al., 2013) and consistent with (Boss and Pegau, 2001; Zhang et al., 2021).

https://doi.org/10.5194/essd-2026-623
Preprint. Discussion started: 21 August 2026

Open Access Earth System Science Data Discussions

3.3.2 Above-water reflectance from So-Rad

Above-water remote-sensing reflectance (R_{rs}) were collected by the So-Rad (, an autonomous, robotic, system which rotates to maintain an optimal viewing geometry relative to the solar azimuth (Jordan et al., 2022, 2023; Wright and Simis, 2021). So-Rad R_{rs} spectra are derived from near-simultaneous measurements of sky radiance (L_s), water radiance (L_t) and downwelling irradiance (E_d) which are measured using TriOS-RAMSES visible-wavelength hyperspectral radiometers at ~ 10 nm spectral resolution and ~ 3 nm native sample spacing. The HSR-1 (Hyperspectral Radiometer) system, which measures E_d, direct (E_{dd}) and diffuse (E_{ds}) downwelling irradiance at a higher spectral resolution (~ 3nm), was installed alongside So-Rad (Jordan et al., 2022; Wood et al., 2017). The data coverage map for So-Rad R_{rs} collected on TARA Europa during 2023 and 2024 (including the additional HyperBOOST-only leg from Greece-France) is shown in Figure 1. In 2023, So-Rad R_{rs} were collected from 04/03/2023 to 02/11/2023. In 2024 So-Rad data were collected from 22/03/2024 (approximately three weeks into the main TREC sampling) to the end of the campaign. HSR-1 data were collected co-incident with So-Rad from 06/06 onwards in 2023, and throughout 2024. In normal operation, So-Rad data were collected continuously at a sample rate of ~ 15 sec, when the solar elevation angle was > 30 degrees. In 2023, there were system issues which resulted in loss of data from the northern European coast, Norway and northern Scotland. From August 2023 onwards, and throughout 2024, there were no significant system issues impacting on data collection.

In this deployment, the So-Rad data were processed using HyperCP; the open-source `Hyper-In-Space Community Processor' (Aurin et al., 2024) with a dedicated branch within HyperCP for the So-Rad system (https://github.com/nasa/HyperCP/tree/So-Rad). HyperCP, which was developed as a validation tool for the NASA PACE mission, provides a full above-water R_{rs} processing chain from Level 0 data (radiance and irradiance in digital numbers) to Level 2 data (reflectance and normalized water-leaving radiance with propagated uncertainties) (Tilstone et al., 2025).The uncertainty budget incorporates uncertainty due to TriOS-RAMSES sensor characteristics (e.g. cosine response, stay-light, non-linearity), calibration, environmental conditions and noise (Vabson et al., 2025). For the bulk processing, the glint (`rho') correction from Mobley *et al.* 1999 the NIR correction from Ruddick et al., 2006), and the BRDF correction from (Lee et al., 2011) were selected as HyperCP Level 2 physics options suitable for optically complex and eutrophic waters. In oligotrophic waters, such as the HyperBOOST leg in August 2024, the NIR correction defaults to no-offset correction, enabling processing with a single configuration for the whole deployment. Quality control was implemented sequentially at different levels within HyperCP. At level 1A (pre-calibration) relative azimuth (between 90 and 140 degrees), tilt (< 5 degs) and windspeed (<8 m/s) filters were applied. At level 1B (calibration to SI units) radiance and irradiance spectra were filtered for outliers, based on spectral variability of hourly measurement bins. At Level 2 (derivation of R_{rs}), data was binned in 5-minute ensemble windows, and a fixed fraction of measurements with the highest upwelling radiance values were removed within each bin (the `glint' filter). To account for the So-Rads' slower sample rate (~15 sec) than a fully continuous above-water system (< 1 sec), we relaxed the fraction of measurements to be removed to be 50% (from a typical default of 10%). This resulted in 6-8 spectra in each measurement bin post QC. As an additional layers of QC, the remaining anomalous spectra were identified and removed using the QWIP score (Dierssen et al., 2022); spectra which had a negative value on the

https://doi.org/10.5194/essd-2026-623
Preprint. Discussion started: 21 August 2026

interval [380,700] nm were also removed. This resulted in a total of 7001 So-Rad R_{rs} spectra binned at 5 minutes available for further analyses.
To summarize the reflectance spectra, the apparent visible wavelength (AVW), a one-dimensional geophysical metric calculated as the weighted harmonic mean of the reflectance spectrum across a range of wavelengths, was used (Vandermeulen et al., 2020). Moreover, based on a simplified classification, the AVW ranges can be used to identify blue-green waters (AVW 400 - 510 nm), green waters (AVW 510 - 590 nm; the brown waters have $R_{rs}(665) > R_{rs}(560)$ AVW ranging from 555 to 575 nm, thus overlapping with the upper end of the green waters (Dierssen et al., 2022).

3.4 Reflectance from the HTSRB system

At selected stations, when the weather and sea-state conditions were favourable, hyperspectral upward radiance (L_u) and downwelling irradiance (E_d) were collected with a Seabird Sci. HTSRB system. HTSRB system data were processed as in (Chase et al., 2017) (Section 2.2). IOPs were used to estimate the attenuation correction of Lu to extrapolate it to the surface as described below.
The data were collected in buoy mode with the HTSRB floating far from the vessel (~100m) measuring tilt and upwelled radiance (L_u) at about 20cm below the surface. A reference radiometer (E_d(0+)) was also installed on the buoy.
Data were processed using the manufacturer software (SatCon, http://www.seabird.com/software/satcon). Immersion coefficients were used in the processing of the upwelled radiance data.
The basic processing steps completed were: i) subtraction time-interpolated E_d dark data from E_d light data; repeat for L_u dark and light; ii) removal of E_d, E_u and L_u spectra that have tilt values above a 5 degrees; and iii) removal of E_d, and L_u spectra that fell outside the middle 50th percentile of E_d data (this removed any outliers in E_d, e.g. from small clouds passing over – data between the 25th and 75th percentiles was retained).

Computation of remotely sensed reflectance (R_{rs}):

R_{rs} (remote-sensing reflectance) is defined as the water-leaving radiance (L_w, i.e. the radiance just above the sea surface) normalized by the downwelling irradiance (E_d):

$$R_{rs}(\lambda) = \frac{L_w(\lambda, 0^+)}{E_d\,(\lambda, 0^+)} \quad \textbf{(9)}$$

In order to compute $L_w(\lambda, 0^+)$ we extrapolated from the depth of the sensor (z=0.2m) and cross the air-water interface:

$$L_w(\lambda, 0^+) = L_u(\lambda, z)\exp\big(z \cdot K_{Lu}(\lambda)\big)\frac{t}{n_{sw}} \quad \textbf{(10)}$$

Where $t = 0.98$ is a transmission coefficient and $n_{sw}$the index of refraction of seawater that we get from Quan and Fry (1995).

https://doi.org/10.5194/essd-2026-623
Preprint. Discussion started: 21 August 2026

The attenuation was computed from IOPs as follows:

$$K_{Lu}(\lambda) = \frac{a_{sw}(\lambda) + a_g(\lambda) + a_p(\lambda) + b_{b,sw}(\lambda) + b_{b,p}(\lambda)}{0.5} \tag{11}$$

The equation to extrapolate L_u to just below the sea surface requires information on the absorption properties of the surface water. The absorption by saltwater ($a_{sw}(\lambda)$) was taken from the recent IOCCG (2018) report augmented with temperature and salinity effects based on Sullivan et al., (2006) and Zhang et al., (2009).

We obtained the absorption and backscattering coefficients due to particulate, $a_p(\lambda)$ and $b_{b,p}(\lambda)$ respectively, and from the inline system, within 15min of the HTSRB measurements (except when not available, see below). For dissolved absorption, we used a relation developed between the inline CDOM fluorescence and discrete measurements of CDOM. Value of particulate IOPs were extrapolated to the UV assuming particulate absorption and backscattering stays at the same value as near 400nm.

For a few dates, we did not have inline $a_p(\lambda)$ in which case we used a chlorophyll-based relationship from TChla to $a_p(\lambda)$ based on Chase et al, 2013, using TChla estimated from R_{rs}. For a few dates we did not inline$b_{b,p}(\lambda)$ in which case we used a relationship between TChla and $b_{b,p}(\lambda)$ from (Morel and Maritorena, 2001) using TChla estimated from R_{rs}. During one station no TSG was available within 15min and was interpolated from measurement further away in time. During one station no DOM fluorescence was available within 15min and was interpolated from measurement further away in time.

3.5 Data Co-location

For the IOP and AOP measurements collected in continuous during the expedition, values were extracted for each station to generate the collocated dataset based on station duration, the CTD deployment time and the station coordinates.

Inline measurements ($a_p(\lambda)$, $c_p(\lambda)$ and $b_{b,p}(\lambda)$), were extracted from daily files and aggregated at the station scale using the CTD deployment time as the temporal reference. For each CTD cast (i.e., each station occurrence), an extraction window ±15 minutes centred on the CTD time was used (total window length = 30 minutes). Within this window, the workflow was applied independently to each inline data stream (AC-S particulate products, HyperBB backscattering, SUVF fluorescence, TSG temperature/salinity, and AC-S derived products). For each instrument/time series all measurements whose timestamps fall within the CTD window (±15 min) were selected. To ensure that the selected measurements correspond to the station location, the latitude/longitude span of the extracted inline measurements was computed and compared against station coordinates from the metadata. Data were retained only if station coordinates fell within the extracted measurement envelope, using a tolerance of approximately ±0.1° in latitude and longitude. For AC-S particulate data, quality flags were used to remove spectra affected by known issues (e.g., bubbles). Flag logic was applied through a binary mask, and flagged spectra were set to NaN prior to computing station statistics.

Remaining spectra were checked for physically unrealistic values, and any spectrum containing negative a_p or cp values was excluded (set to NaN). Finally, for each station and for each wavelength-

https://doi.org/10.5194/essd-2026-623
Preprint. Discussion started: 21 August 2026

dependent variable, the station value was computed as the median of all retained spectra within the CTD window. Associated uncertainty is defined calculated as the standard deviation of the selected spectra. R_{rs} spectra from So-Rad (and similarly from HTSRB) daily files were associated with Tara stations using station metadata (date, time, and position) through a hierarchical extraction procedure designed to maximize temporal and spatial consistency between radiometric and in situ measurements. For each station and date-matched R_{rs} file, spectra were selected according to four successive criteria. First, when CTD time information was available, spectra acquired within ±30 minutes of the CTD sampling time were selected. A spatial consistency check was then applied by retaining only spectra located within ±0.1° latitude/longitude of the station coordinates when such matches were available. If no spectra satisfied the CTD-based criterion, spectra acquired within the station time window (between the station start and end times reported in the Tara metadata) were selected, again with the same coordinate-based refinement when possible. If no spectra were found within the station sampling period, the selection was extended to spectra acquired within ±1 hour of the station start or end times, followed by the same spatial filtering. As a final fallback, when no robust temporal match was identified, all spectra from the date-matched daily file were associated with the station. For each station, the selected spectra were stored along with extraction-quality flags indicating the selection method used (CTD-centered, station-time, extended-time, or date-only association) and whether coordinate filtering refined the final selection. The station-associated R_{rs} spectrum was then calculated as the median of all selected spectra at each wavelength, while the associated uncertainty was estimated as the standard deviation of the selected spectra.

3.6 Optical closure assessments

As presented above and reported in Table 1, several variables were acquired with different instruments and methods. Some of these quantities were measured in the lab by using water samples, as well as by the line instruments, such as the absorption coefficients measured and derived with AC-S and from discrete measurements. Similarly, above and in-water radiometry were collected with So-Rad and HTSRB. This provides an opportunity to assess the internal consistency of the whole dataset by performing several optical closure assessments.
To this aim the agreement between the reference spectrum ($x_i(\lambda)$) and the comparison spectrum ($y_i(\lambda)$), where i denotes the station number, was evaluated for each wavelength (λ), using the signed percent difference (SPD), absolute percent difference (APD), coefficient of determination (r^2), and the type-II regression slope (S) with 1-sigma uncertainty bounds.

$$APD_i(\lambda) = 100 \cdot \left|\frac{y_i(\lambda) - x_i(\lambda)}{x_i(\lambda)}\right| \quad (12)$$

$$SPD_i(\lambda) = 100 \cdot \left(\frac{y_i(\lambda) - x_i(\lambda)}{x_i(\lambda)}\right) \quad (13)$$

https://doi.org/10.5194/essd-2026-623
Preprint. Discussion started: 21 August 2026

$$r^2(\lambda) = \left(\frac{\sum_{i=1}^{n} \left(x_i(\lambda) - \overline{x}(\lambda)\right)\left(y_i(\lambda) - \overline{y}(\lambda)\right)}{\sqrt{\sum_{i=1}^{n} \left(x_i(\lambda) - \overline{x}(\lambda)\right)^2} \cdot \sqrt{\sum_{i=1}^{n} \left(y_i(\lambda) - \overline{y}(\lambda)\right)^2}} \right)^2 \quad \textbf{(14)}$$

$$s(\lambda) = \frac{S_y(\lambda)}{S_x(\lambda)} \quad \textbf{(15)}$$

$S_y(\lambda)$ and $S_x(\lambda)$ represent $x(\lambda)$ and $y(\lambda)$ standard deviations. For each wavelength, the distributions of $APD_i(\lambda)$ and $SPD_i(\lambda)$ across stations were summarized using the median and the interquartile range.

4 Dataset overview

The HyperBOOST hyperspectral dataset acquired in 2023 and 2024 during the Tara Europa Expedition across the major European seas is available at https://doi.org/10.5281/zenodo.18340674 (Costanzo et al., 2026b) in tabular form and contains collocated in situ data collected at discrete stations and those acquired continuously. The number of available measurements for each variable is reported in Table 2, POC, DOC, a_{phy}, a_{NAP}, and a_{CDOM} were available at all 202 stations. After co-location to the 202 stations, continuous HyperBB (b_{bp}) and AC-S data (a_p and c_p) were available for 171 and 164 stations, respectively. Concerning radiometric data, a total of 128 R_{rs} spectra were available for the So-Rad and 45 for the HTSRB. The spatial coverage of the continuous IOPs and radiometry data is presented in Figure 1. In all tables and figures, the regions will be presented in chronological order of sampling.

Table 2 Number of samples collected for the bio-optical and hydrographic variables of the HyperBOOST collocated dataset.

N	sal	TChla	SPM, POF	POC, DOC, a_{phy}, a_{NAP}, a_{CDOM}	b_{bp}	a_p /c_p AC-S	R_{rs} So-Rad	R_{rs} HTSRB
All	201	198	197	202	164	171	128	45
English Channel	9	9	9	9	7	8	4	2
North Sea	22	22	22	22	20	21	5	0
Skagerrak-Kattegat	16	16	16	16	15	16	4	1
BalticSea	23	23	23	23	21	23	15	0
Atlantic Coast	28	28	29	29	20	18	18	10
Western Mediterranean Sea	19	19	19	19	17	15	2	7
Gulf of Lion	8	8	8	8	5	7	6	1
Tyrrhenian Sea	25	25	25	25	22	21	24	4
Adriatic Sea	21	19	17	21	19	16	21	10

https://doi.org/10.5194/essd-2026-623
Preprint. Discussion started: 21 August 2026

Eastern Mediterranean Sea	30	29	29	30	18	26	29	10

Table 3 reports the summary statistics of the quantities describing bio-optical and hydrographic characteristics of the HyperBOOST collocated dataset. Table 4 presents the median and inter quartile ranges for the main bio-optical quantities to highlight the biogeochemical variability within and across the sampled regions.

Figure 2 presents the distribution of the CDOM, SPM and TChla for the stations sampled during the whole expedition. The SPM concentration ranged ~0.04–200 mg L^{-1} (median 0.88 mg L^{-1}, Table 3), the maximum concentrations were found inside the macrotidal estuaries along the French Atlantic coasts (off the Loire and Gironde Rivers) while the lowest values were sampled in the offshore oligotrophic waters of the Tyrrhenian and Ionian Sea during the return leg. The highest regional median SPM values were observed in the Atlantic Coast and Baltic Sea (1.74 and 1.72 g m^{-3}, respectively), while the lowest were found in the Eastern Mediterranean Sea (0.24 g m^{-3}, Table 4). The organic fraction varied from 8.7% in estuaries to 100% in offshore oligotrophic waters (Table 3). $a_{CDOM}(443)$ ranged ~0.01–2.1 m^{-1}, with the higher median values sampled in the Baltic Sea and North Sea (0.51 and 0.27 m^{-1}, respectively, Table 4). Overall, the *aCDOM(443)* values sampled in the Mediterranean in 2024 showed a lower range across all sub-basins, with an absorption consistently lower than ~0.2 m^{-1}, with the only exception of the Adriatic Sea and a couple of stations in the Gulf of Lion. TChla ranged ~0.03–24.2 mg m^{-3}, with the higher values occurring in the English Channel, where a spring bloom was sampled in April 2023, reflected also in the largest interquartile range across all regions (18.61 mg m^{-3}, Table 4). The highest median values were sampled in the Baltic Sea and North Sea (5.19 and 2.27 mg m^{-3}, respectively), while the lowest median values were observed in the Eastern Mediterranean and Tyrrhenian Seas (0.12 and 0.25 mg m^{-3}, respectively, Table 4). The $a_{CDOM}(443)$, SPM and TChla ranges reported for this dataset were comparable to those reported within European waters in the BiOMaP, COASTℓOOC and COASTCOLOUR datasets (Babin et al., 2003b, a; Nechad et al., 2015; Zibordi and Berthon, 2024).

DOC covered a wider range than POC (51–679 µM and 1–80 µM respectively, Figure 3 and Table 3). Overall, POC showed relatively low variability across most regions, with the notable exception of the Baltic Sea, which had the highest median value (33.51 µM, Table 4), and the Skagerrak-Kattegat, which showed the lowest median (5.44 µM). Notably, the Eastern Mediterranean showed a comparatively elevated POC median (22.34 µM) despite its oligotrophic character. These POC values were comparable to the ranges and spatial distribution reported for the European in the COASTℓOOC dataset (Babin et al., 2003b; Massicotte et al., 2023). DOC displayed large variability across regions, with the highest median concentrations observed in the Baltic Sea and the Skagerrak-Kattegat (398 and 226 µM, respectively), while the lowest median values were found in the Western Mediterranean and Tyrrhenian Seas (61 and 67 µM, respectively, Table 4). The DOC ranges observed during the expedition were comparable with global observations: the CoastDOM dataset (Lønborg et al., 2024) reported average ±standard deviation of 182 ±314 µM and a median values 103 µM and noted that DOC ranging between 300 and 600 µM were predominantly collected in eutrophic and river-influenced coastal waters of the

https://doi.org/10.5194/essd-2026-623
Preprint. Discussion started: 21 August 2026

Northern Hemisphere, such as the Baltic Sea. Moreover, the DOC ranges observed in 2024 across the five sub-basins were comparable with the mean concentrations ranging between 57 and 101 µM reported for the Mediterranean Sea by Santinelli (2015).

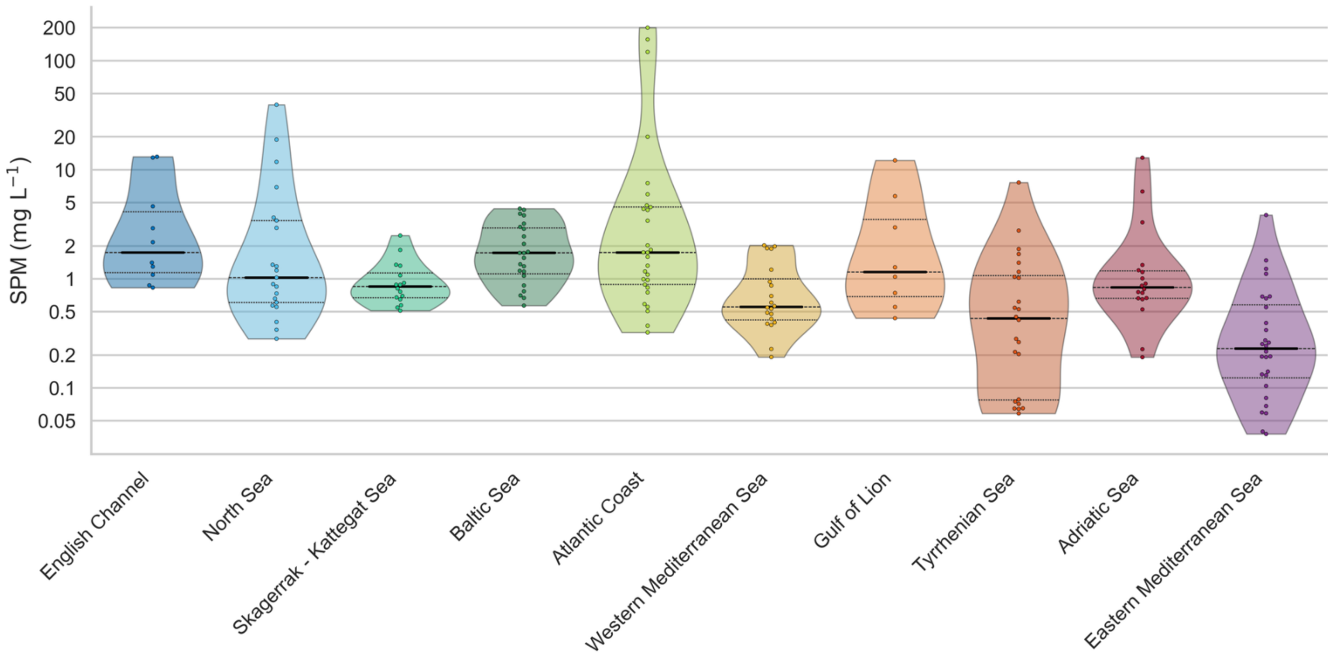

https://doi.org/10.5194/essd-2026-623
Preprint. Discussion started: 21 August 2026

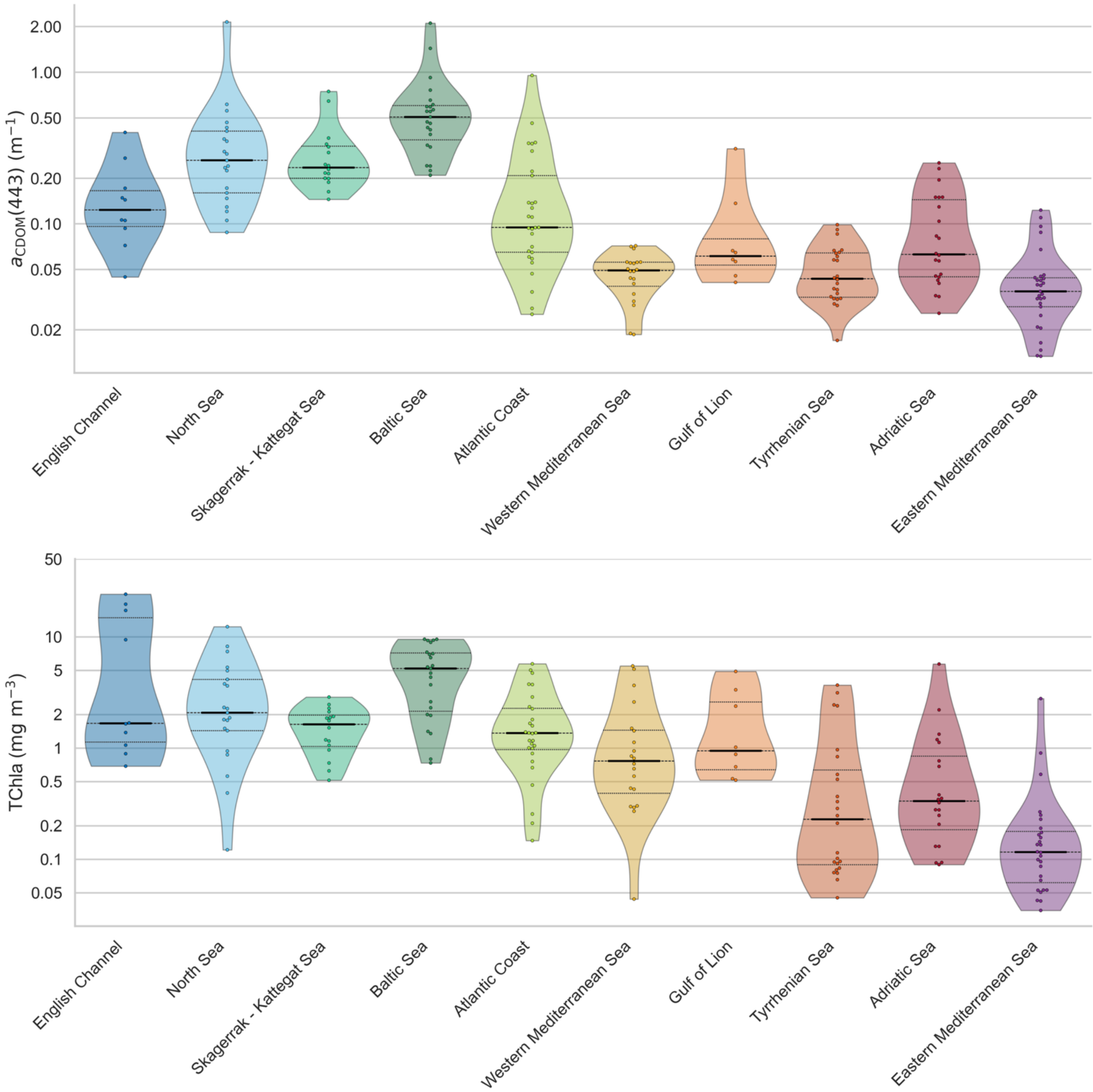

Figure 2. Overview of the SPM, $a_{CDOM}(443)$ and TChla distribution for the stations sampled during the Tara Europa Expedition. In the three panels, the regions are colour coded consistently with Figure 1. The violin plots report the measurements as dots; the bold black bars mark the median values; the distribution of data is represented by the shape of the violin.

https://doi.org/10.5194/essd-2026-623
Preprint. Discussion started: 21 August 2026

Open Access
Earth System Science Data
Discussions

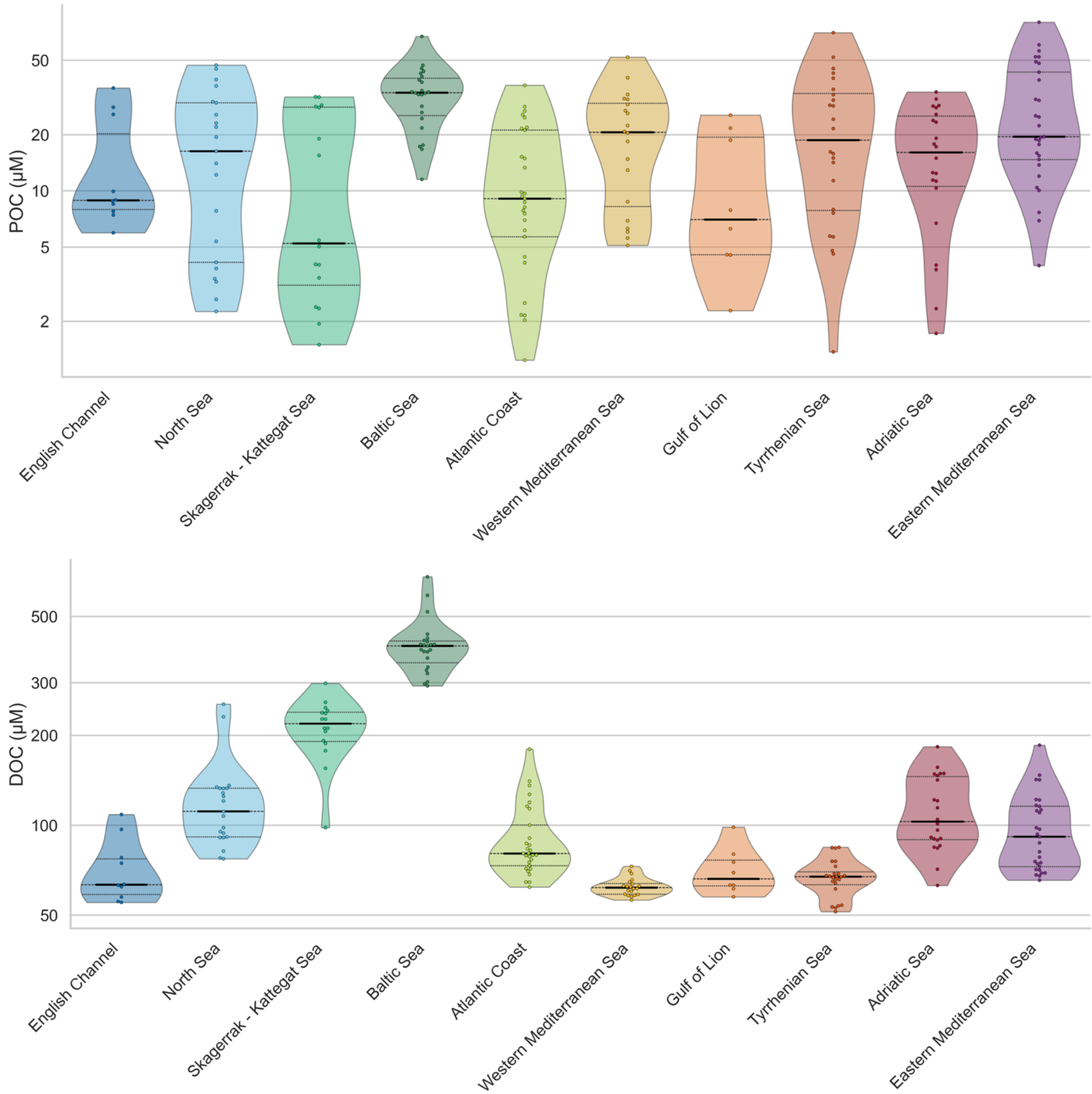

Figure 3. Overview of the POC and DOC distribution for the stations sampled during the Tara Europa Expedition. In the two panels, the regions are colour coded consistently with Figure 1. The violin plots report the measurements as dots; the bold black bars mark the median values; the distribution of data is represented by the shape of the violin.

https://doi.org/10.5194/essd-2026-623
Preprint. Discussion started: 21 August 2026

Table 3 Summary statistics of the quantities describing bio-optical and hydrographic characteristics of the HyperBOOST collocated dataset

	N	avg	std	min	25th	median	75th	max	IQR
sal	201	30.3	10.7	4.1	28.1	34.9	37.7	40.8	9.6
TChla	198	2.12	3.26	0.03	0.27	0.99	2.38	24.18	2.12
SPM	197	4.38	20.07	0.04	0.51	0.88	1.84	200.28	1.34
POF	197	58.27	25.19	8.73	37.26	56.48	78.73	100.00	41.47
POC	202	20.46	15.27	1.24	7.61	17.83	30.03	80.06	22.42
DOC	202	135.14	110.91	51.33	68.44	89.21	142.18	678.77	73.74
$a_{nw}(443)$	202	0.3826	0.6671	0.0187	0.0736	0.1823	0.4172	5.3789	0.3435
$a_{phy}(443)$	202	0.0581	0.0695	0.0008	0.0133	0.0358	0.0740	0.4239	0.0607
$a_{CDOM}(443)$	202	0.1924	0.2803	0.0134	0.0440	0.0878	0.2406	2.1467	0.1966
$a_{NAP}(443)$	202	0.1321	0.5041	0.0011	0.0090	0.0294	0.0762	4.3433	0.0672
$b_{bp}(560)$	164	0.0527	0.2654	0.0003	0.0025	0.0061	0.0144	2.0387	0.0120
$c_p(660)$	171	2.2245	3.7891	0.0808	0.3933	1.0618	2.2993	31.4885	1.9060

https://doi.org/10.5194/essd-2026-623
Preprint. Discussion started: 21 August 2026

Table 4 Median and Interquartile ranges of the main bio-optical quantities for the HyperBOOST regions

	All	English Channel	North Sea	Skagerrak-Kattegat	Baltic Sea	Atlantic Coast	Western Mediterranean Sea	Gulf of Lion	Tyrrhenian Sea	Adriatic Sea	Eastern Mediterranean Sea
sal	34.9, 9.6	34.5, 1.0	32.4, 5.7	19.9, 7.7	6.1, 1.8	35.0, 3.2	38.1, 0.6	36.6, 2.6	38.1, 1.2	35.9, 5.6	38.6, 3.9
TChla	0.99, 2.12	1.65, 18.61	2.27, 3.88	1.76, 1.06	5.19, 6.93	1.37, 1.36	0.72, 2.29	0.88, 2.66	0.25, 0.88	0.35, 0.98	0.12, 0.13
SPM	0.88, 1.34	1.40, 3.52	1.19, 6.30	0.88, 0.64	1.72, 2.14	1.74, 3.82	0.54, 1.49	1.27, 4.68	0.45, 1.08	0.86, 0.67	0.24, 0.53
POF	56.48, 41.47	40.52, 25.53	55.16, 58.77	87.16, 26.56	76.45, 35.99	36.43, 31.65	54.20, 25.25	29.33, 29.75	68.89, 51.28	47.65, 27.25	64.98, 50.68
POC	17.83, 22.42	8.94, 20.29	16.33, 25.88	5.44, 24.87	33.51, 18.22	9.09, 15.88	20.81, 22.44	6.92, 14.14	21.57, 27.04	14.96, 15.31	22.34, 33.52
DOC	89.21, 73.74	62.95, 20.39	111.17, 41.54	226.46, 49.93	398.50, 84.39	80.42, 40.34	61.34, 6.97	64.49, 17.05	67.42, 11.33	104.58, 58.38	91.48, 45.26
a_{nw}(443	0.1823, 0.3435	0.1869, 0.3923	0.5282, 0.6338	0.3699, 0.1390	0.7596, 0.6163	0.2822, 0.3708	0.0931, 0.0485	0.1436, 0.3297	0.0779, 0.0844	0.0942, 0.1748	0.0500, 0.0334
$a_{phy}(443)$	0.0358, 0.0607	0.0453, 0.0715	0.0712, 0.0578	0.0538, 0.0304	0.1342, 0.1166	0.0547, 0.0503	0.0316, 0.0276	0.0348, 0.0540	0.0097, 0.0151	0.0182, 0.0462	0.0059, 0.0060
$a_{CDOM}(443)$	0.0878, 0.1966	0.1060, 0.0783	0.2712, 0.2712	0.2419, 0.1355	0.5075, 0.3240	0.0947, 0.1570	0.0486, 0.0215	0.0581, 0.0813	0.0440, 0.0318	0.0637, 0.1045	0.0358, 0.0166
$a_{NAP}(443)$	0.0294, 0.0672	0.0567, 0.1238	0.0517, 0.3001	0.0456, 0.0537	0.0630, 0.1833	0.0768, 0.1925	0.0094, 0.0102	0.0642, 0.1856	0.0115, 0.0444	0.0180, 0.0194	0.0049, 0.0067
$b_{bp}(560)$	0.0061, 0.0120	0.0112, 0.1030	0.0095, 0.0737	0.0070, 0.0139	0.0221, 0.0242	0.0063, 0.0368	0.0024, 0.0021	0.0140, 0.0742	0.0030, 0.0069	0.0050, 0.0072	0.0010, 0.0013
$c_p(660)$	1.0618, 1.9060	1.4669, 2.4268	1.8332, 6.4507	1.4763, 1.1606	3.1513, 3.1187	1.1399, 4.2612	0.4575, 0.5723	1.5619, 21.7265	0.3368, 1.3700	0.9892, 0.9792	0.2492, 0.2474

https://doi.org/10.5194/essd-2026-623
Preprint. Discussion started: 21 August 2026

4.1 Inherent optical properties

Figure 4 provides an overview of the IOPs continuous measurements collected during the expedition and the results of the co-location procedure of the IOPs at the station locations. The temporal variability of the inline $a_p(443)$, $b_{bp}(560)$, and $c_p(660)$ captured by the dataset reflects the sampling strategy, which typically involved offshore, mid-distance, and near-shore transects within each region. The values extracted at the station locations are often within the daily box-plot of the continuous measurements presenting the daily medians, 25th and 75th percentiles. In several instances the extracted values lie above or below the boxplot; this occurred when higher values were measured in the near-shore stations (or lower values for the offshore stations) compared to transects acquired during the rest of the day.
For 2023, a_p(443) spanned approximately 0.01 to >1 m^{-1}, with the North Sea transects showing intermediate values with high variability, followed by a decrease in the Skagerrak-Kattegat, and an increase in the Baltic Sea where consistently high values and relatively low daily box-plot spread were observed. After the Baltic Sea, intermediate and more variable values were recorded again in the North Sea, with the oscillating pattern and high variability maintained throughout the Atlantic Coast transects. Here, values started to be generally lower compared to the Baltic Sea and English Channel. The $b_{bp}(560)$ ranged from ~0.005 to >0.1 m^{-1} and followed a broadly similar pattern across regions; three distinct and prominent peaks were observed in late September during the Atlantic Coast transect, standing out clearly from all other values. The $c_p(660)$ ranged from ~0.1 to >10 m^{-1} and showed a behaviour broadly similar to $a_p(443)$, with intermediate values and high variability in the North Sea, a decrease in the Skagerrak-Kattegat, consistently high values in the Baltic Sea, and an oscillating pattern with high variability in the subsequent North Sea and Atlantic Coast transects, though with an overall somewhat narrower dynamic range compared to $a_p(443)$.
In 2024, the temporal coverage extended from February through August, and the overall dynamic range of all three parameters was reduced compared to 2023. The $a_p(443)$ spanned ~0.01 to ~0.4 m^{-1}, the $b_{bp}(560)$ ranged from ~0.001 to ~0.03 m^{-1}, and $c_p(660)$ reached at most ~2–3 m^{-1}, with the latter showing the largest relative drop compared to 2023 where values exceeded 10 m^{-1}. The $a_p(443)$ showed lower values (~0.01–0.05 m^{-1}) in the Western Mediterranean at the start of the leg, intermediate values with higher variability (~0.05–0.2 m^{-1}) during the Gulf of Lion and Tyrrhenian transects, a prominent peak (~0.3–0.4 m^{-1}) at the beginning of June during the Adriatic Sea transects, followed by generally lower values (~0.01–0.1 m^{-1}) with some higher excursions during the Eastern Mediterranean homeward leg. The $b_{bp}(560)$ followed a broadly similar pattern, with low values (~0.001–0.005 m^{-1}) in the Western Mediterranean, intermediate values with higher variability (~0.005–0.02 m^{-1}) in the Gulf of Lion and Tyrrhenian transects, a peak (~0.02–0.03 m^{-1}) at the beginning of June during the Adriatic Sea transects, and a decrease towards the end of the time series in the Eastern Mediterranean. The $c_p(660)$ showed a consistent pattern, with low values (~0.1–0.5 m^{-1}) in the Western Mediterranean, intermediate values with higher variability (~0.5–1.5 m^{-1}) in the Gulf of Lion and Tyrrhenian transects, a peak (~2–3 m^{-1}) during the Adriatic Sea transects, and generally low values (~0.1–0.3 m^{-1}) towards the end of the leg in the Eastern Mediterranean.

https://doi.org/10.5194/essd-2026-623
Preprint. Discussion started: 21 August 2026

Overall, $a_p(443)$ ranged ~0.001–0.42 m^{-1} with a median of 0.036 m^{-1} (Table 3), with the highest median values observed in the Baltic Sea and North Sea (0.134 and 0.071 m^{-1}, respectively) and the lowest in the Eastern Mediterranean and Tyrrhenian Seas (0.006 and 0.010 m^{-1}, respectively, Table 4). The $b_{bp}(560)$ spanned ~0.0003–2.02 m^{-1} (median 0.006 m^{-1}, Table 3), with the highest median values in the Baltic Sea and Gulf of Lion (0.023 and 0.014 m^{-1}, respectively) and the lowest in the Eastern Mediterranean and Western Mediterranean Seas (0.001 and 0.002 m^{-1}, respectively, Table 4). Similarly, $c_p(660)$ ranged ~0.10–31.49 m^{-1} (median 1.09 m^{-1},Table 3), with the Baltic Sea and Gulf of Lion showing the highest median values (3.15 and 1.56 m^{-1}) and the Eastern and Western Mediterranean Seas the lowest (0.27 and 0.46 m^{-1}, respectively, Table 4). Across all three parameters, the largest interquartile ranges were found in regions such as the Atlantic Coast and Gulf of Lion, reflecting the high spatial heterogeneity encountered along near-shore transects in these areas.

https://doi.org/10.5194/essd-2026-623
Preprint. Discussion started: 21 August 2026

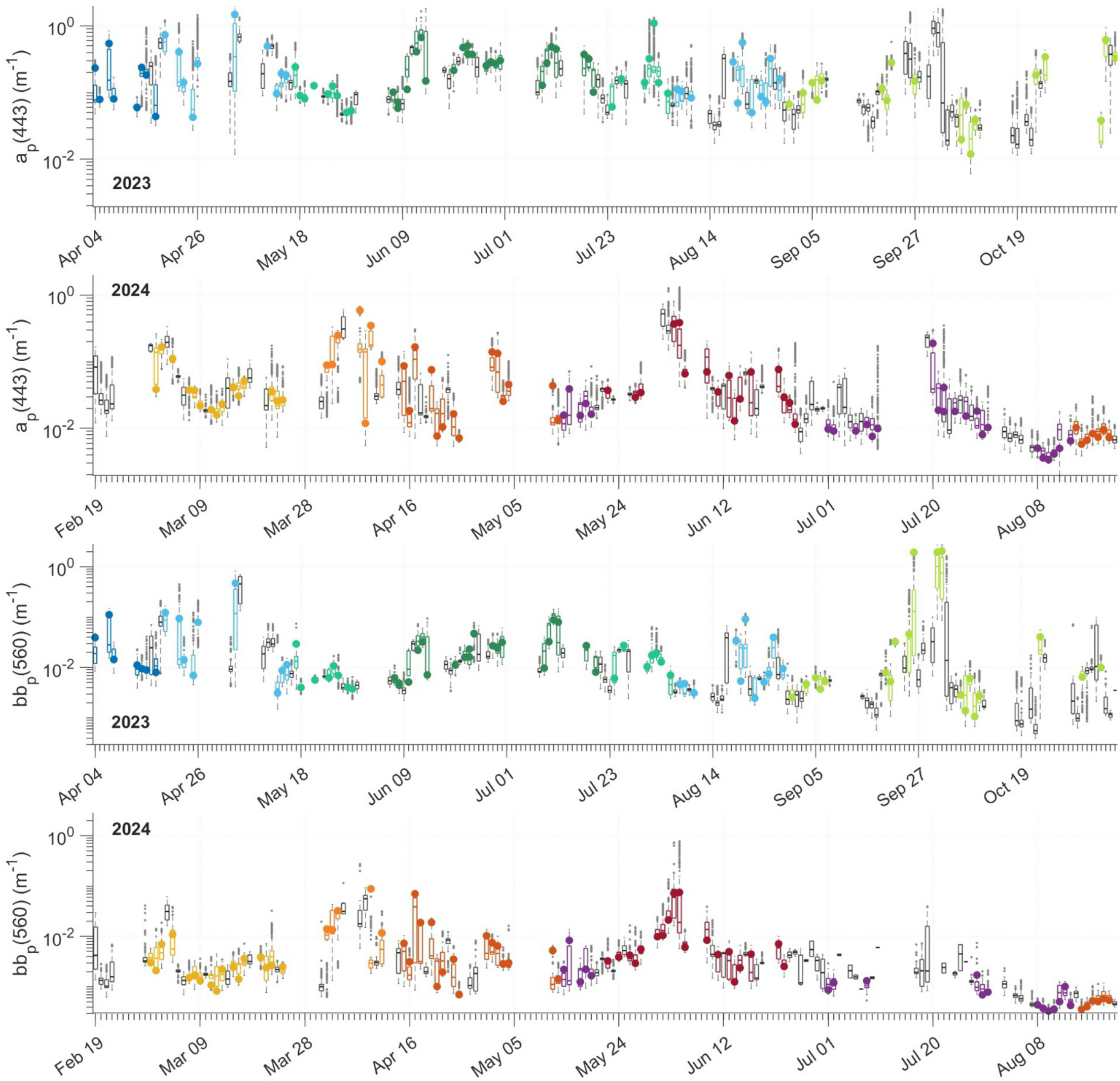

https://doi.org/10.5194/essd-2026-623
Preprint. Discussion started: 21 August 2026

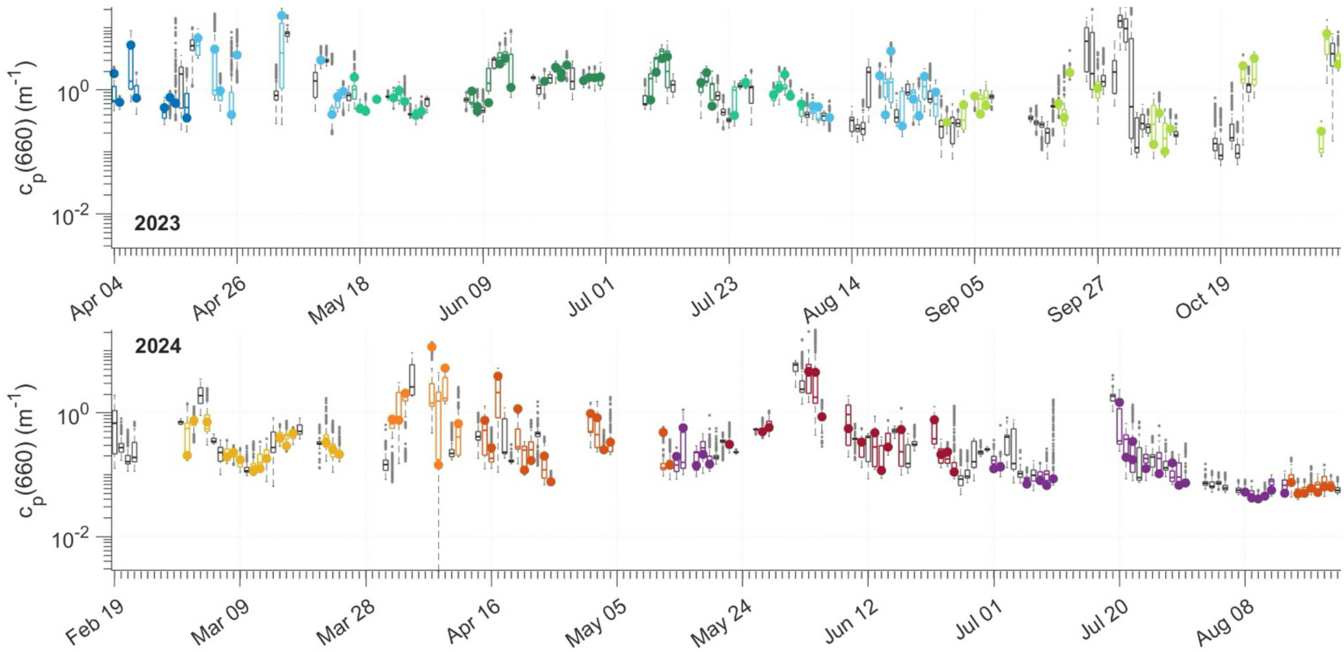

Figure 4 Summary of inline IOP measurements for 2023-2024 Tara Europa Expedition. The dots represent the inline $a_p(443)$ $bb_p(560)$, and $c_p(660)$ extracted for each station, colour coded consistently with Figure 1. The daily distribution the inline IOP are presented with the box plots with daily medians, 25th and 75 percentiles. The box plots are colour coded consistently with Figure 1 for days when a station was sampled, otherwise are black.

4.2 RRS for stations: HTSRB and So-Rad

After co-location to the 202 stations, a total of 128 and 45 R_{rs} spectra were available for the So-Rad and HTSRB, respectively (Table 2, Figure 1). Figure 5 presents the HTSRB and the So-Rad *Rrs* spectra extracted for each station for each sub-basin. The optical variability across the sub-basins clearly emerges from these hyperspectral *Rrs* spectra with dark absorbing waters occurring in the Baltic and Skagerrak - Kattegat with R_{rs}(350-450)<0.002 sr^{-1} and AVW ranging 500-560nm, brown waters (*sensu* Dierssen et al., 2022) with R_{rs}(650-650)>0.015 sr^{-1} and AVW > 530 nm occurring across several regions in resuspension zones and in front of the river mouths, clear blue waters with R_{rs}(600-700) <0.001 sr^{-1} and AVW<480 nm occurring mostly across the Mediterranean sub-basins, reaching AVW<465 nm in the oligotrophic offshore stations of the Eastern Mediterranean and Tyrrhenian Sea sampled in August 2024

The different availability of *Rrs* spectra across the regions (Table 2, Figure 5) is due to some So-Rad outages in early 2023 and deployment in late March 2024, and the HTSRB deployment protocol as the HTSRB was deployed only in 13 and 32 stations in 2023 and 2024 due to the need for cloud-free sky and calm sea surface conditions.

Figure **6** shows the variability in the 7001 So-Rad R_{rs} spectra, acquired continuously, using the AVW calculated from the reflectance spectra (Vandermeulen et al., 2020). As for the IOPs (Figure **4**), the

https://doi.org/10.5194/essd-2026-623
Preprint. Discussion started: 21 August 2026

AVW values extracted at the station location is often within the daily box-plot of the continuous measurements presenting the daily medians, 25th and 75th percentiles.
The optical variability along the track highlights that in the Baltic and Skagerrak – Kattegat the high median values of AVW (500-560nm) and the offshore clear blues waters were characterised by AVW<480 nm were associated with low interquartile ranges. In the resuspension zones and in front of the river mouths the green or brown waters (*sensu* Dierssen et al., 2022) with high median values of AVW (>530 nm) were associated with high interquartile ranges and also with the extracted station values above or below the boxplot, confirming the high spatial heterogeneity observed also for the in-line IOPS in these dynamic areas (Figure 4).

https://doi.org/10.5194/essd-2026-623
Preprint. Discussion started: 21 August 2026

Open Access Earth System Science Data Discussions

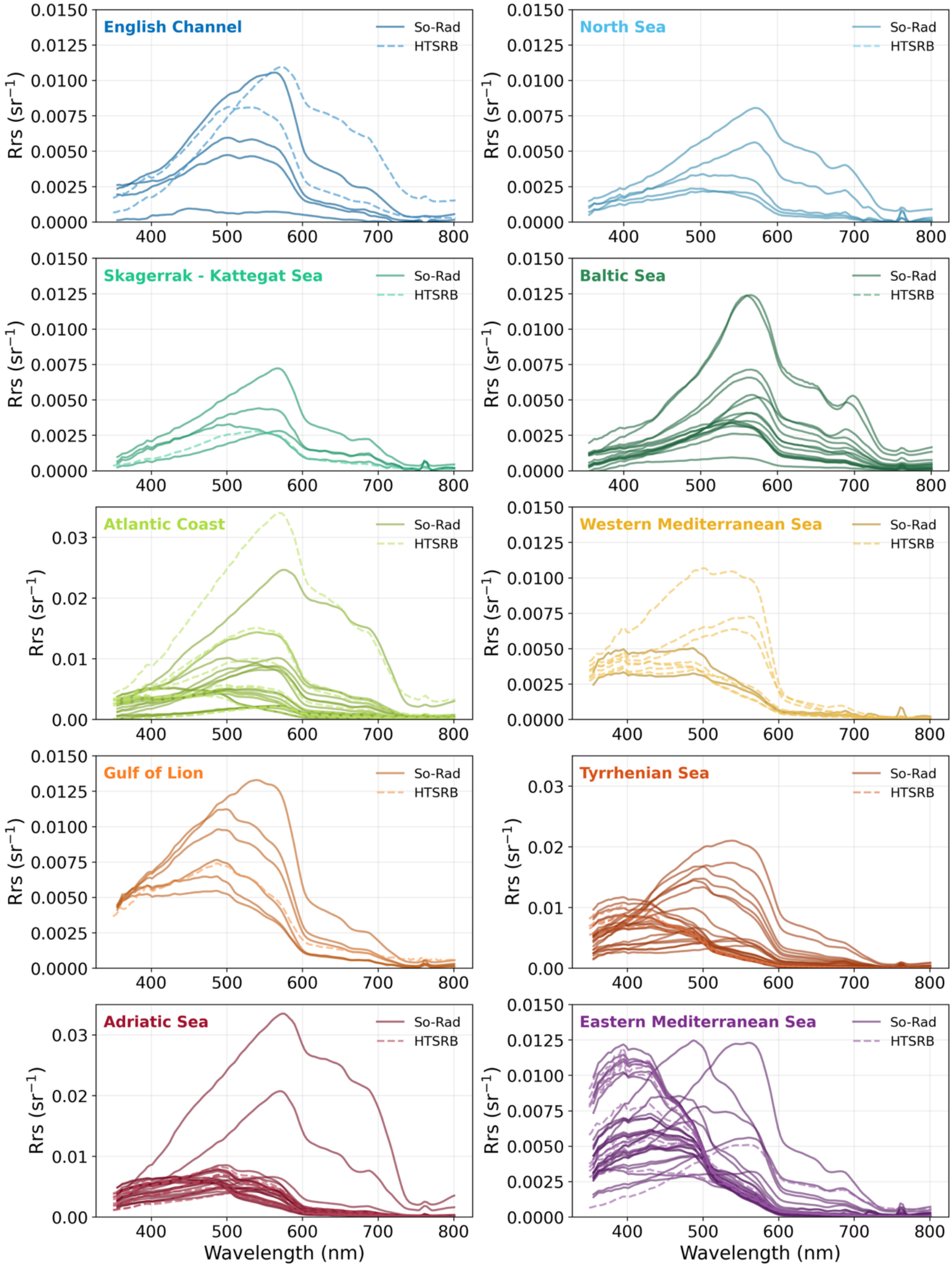

587

https://doi.org/10.5194/essd-2026-623
Preprint. Discussion started: 21 August 2026

Figure 5. Overview of R_{rs} spectra across regions collected at HyperBOOST stations. In the panels, the regions are colour coded consistently with Figure 1. So-Rad and HTSRB spectra are plotted as continuous and dashed lines, respectively. The ranges for Y axes vary, most regions range 0-015 sr^{-1}, Atlantic Coast, Tyrrhenian and Adriatic Sea range 0-0.30 sr $^{-1}$.

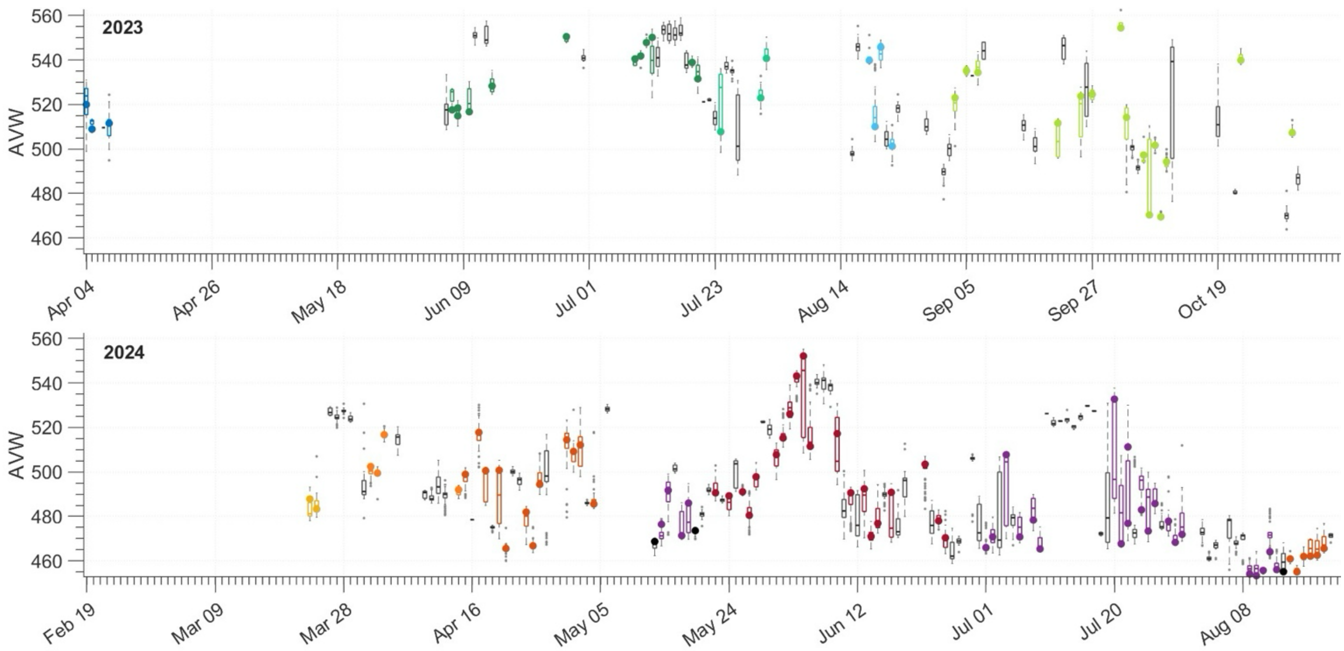

Figure 6. Summary of continuous AOP measurements for 2023-2024 Tara Europa Expedition. The dots represent the AVW for the So-Rad R_{rs} spectra extracted for each station presented in Figure 5, colour coded consistently with Figure 1. The daily distributions for the AVW are presented with the box plots with daily medians, 25th and 75th percentiles. The box plots are colour coded consistently with Figure 1 for days when a station was sampled, otherwise are black.

4.3 Ternary budget

Figure 7 presents the ternary plot of absorption budget at 443 nm combining the co-located a_{phy} and a_{NAP} with the a_{CDOM} for the stations sampled in 2023 and 2024 on the Tara Europa Expedition. At first glance, it can be observed that the stations sampled in 2023 and 2024 cover the full range for the a_{NAP} axis, extending the range reported for european waters in previous studies (Babin et al., 2003b; Zibordi and Berthon, 2024), while the top portion of the plot, where the absorption is dominated by a_{phy} is not fully populated. In Figure 7 is possible to identify stations where the absorption is dominated by non-algal particles (a_{NAP} > 50% of a_{nw}) occurring in the coastal waters of the Atlantic, North and Adriatic seas, while the stations where a_{nw} was dominated by CDOM (a_{CDOM} > 50% of a_{nw}, reaching up to ~95%) occur in the Baltic Sea (70-90%), including also the Skagerrak and Kattegat Sea, similarly to Babin et al. (2003), and also several stations across the Mediterranean Sea sub-basins as in Zibordi and Berthon (2024). The stations dominated by CDOM (a_{CDOM} 70-90% of a_{nw}), where characterized by high

https://doi.org/10.5194/essd-2026-623
Preprint. Discussion started: 21 August 2026

Earth System Science Data
Open Access Discussions

a_{nw} values (up to ~ 5 m^{-1}) as well as the low a_{nw} values (<1.5 m^{-1}). The stations where a_{NAP} > 50% of a_{nw} occurring in the coastal waters of the Atlantic, North and Adriatic seas are characterized by the highest b_{bp} values, and that most of the stations dominated by CDOM (a_{CDOM} 70-90% of a_{nw}) were characterized by low b_{bp} values.

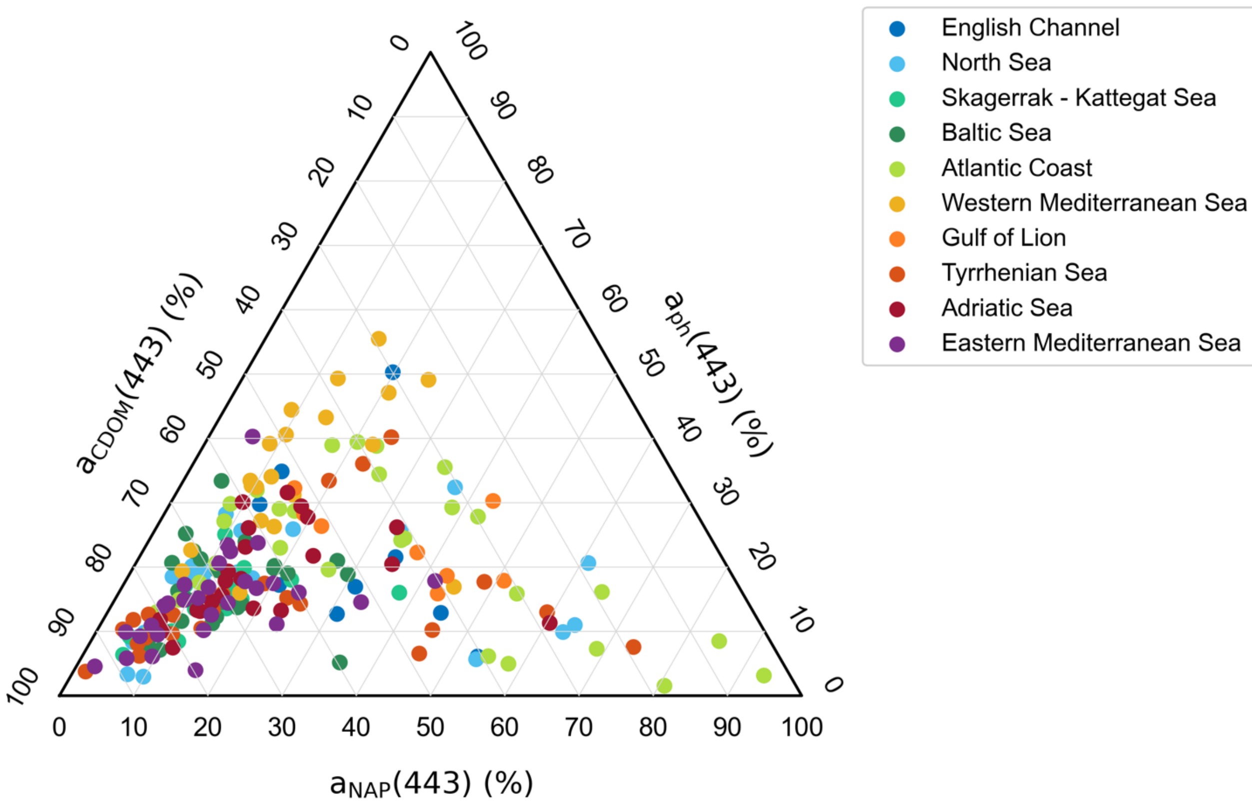

Figure 7 Ternary plot of the absorption budget at 443 nm for stations sampled in 2023 and 2024 on the Tara Europa Expedition.

5 Internal consistency of the dataset

This section presents an assessment of the internal consistency of the dataset by performing optical closure assessments for co-located variables.

Figure 8 and Figure 9 present the comparison of the a_p values measured in the lab from samples and by the in-line AC-S at 145 station locations. Overall, the two approaches cover adequately the same dynamic range for the three selected spectral bands (443, 550, and 676 nm) with some variability around the 1:1 line and at the lower and higher bounds of the range (Figure 8). This good agreement is confirmed by the spectral closure metrics (Figure 9) show a MAPD<25% between 400-700nm, high

https://doi.org/10.5194/essd-2026-623
Preprint. Discussion started: 21 August 2026

correlation (R^2>0.7) between 450 and 700 nm, reaching correlation R>0.8 between 650 and 690 nm. The regression slope is within 0.8 and 1.2 between 450 and 650 nm.

The differences between a_p values measured in the lab from samples and by the in-line AC-S are likely due to some spatial and temporal differences between the measurements by the inline system and the water sampling, the data extraction of the collocation procedure, and the correction procedures applied to the AC-S (e.g. incomplete correction for the detector acceptance angle effects and/or the scattering correction residuals for non- negligible absorption of particles in the NIR) and the lab spectrophotometric measurements. Furthermore, these residuals are overall comparable with those reported by (Zibordi and Berthon, 2024) for their stations.

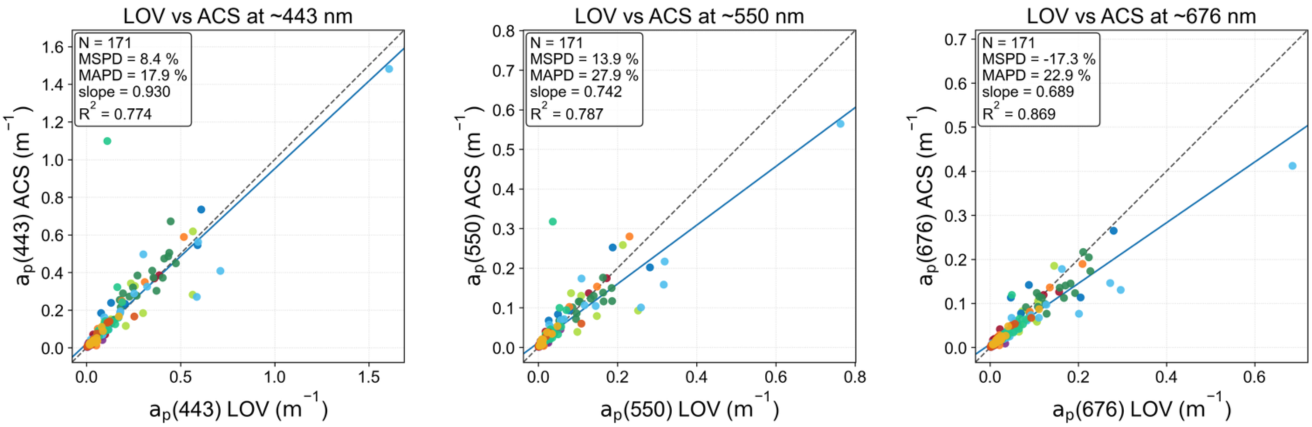

Figure 8: Comparison of the particulate absorption coefficient a_p for stations sampled on the Tara Europa Expedition measured in the lab from samples and by the in-line AC-S.

https://doi.org/10.5194/essd-2026-623
Preprint. Discussion started: 21 August 2026

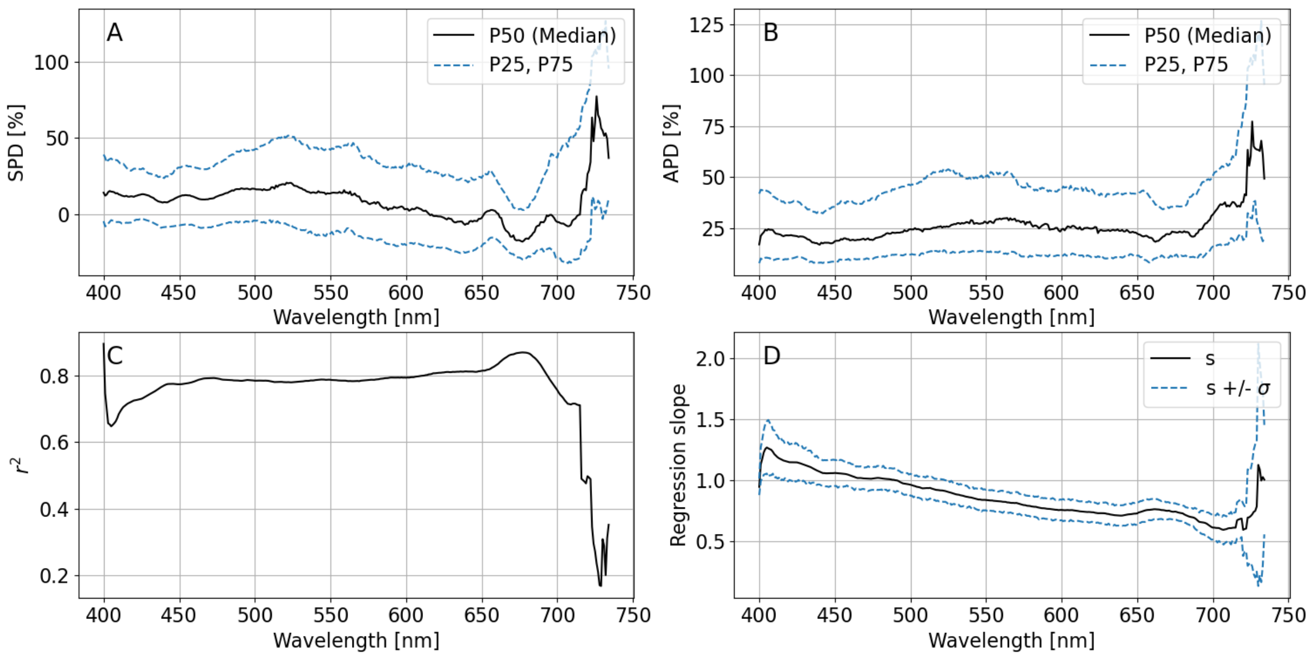

Figure 9: Spectral closure metrics for the comparison of the particulate absorption coefficient $\boldsymbol{a_p}$: A. Median and quartiles for signed percentage difference (SPD) and. B. Absolute percentage difference (APD). C. r^2. D. Regression slope (s) with 1-sigma uncertainty bounds

For the co-location between So-Rad and HTSRB R_{rs} (Figure 10 and Figure 11) we used the closest So-Rad measurement bin to the HTSRB within a maximum tolerance of +/- 30 minutes. The plots for the for 9 OLCI central wavelengths (Figure 10 – see legend and caption for metrics) show overall, the two radiometric approaches were consistent across the dynamic range captured in the 26 stations. The spectral closure metrics (Figure 11) showed high correlation across the whole spectral range, R^2> 0.85 between 350-450 and 510-700nm, MAPD lower than 15 % between 350 and 580 nm. The correlation dip for R^2at 450-500 nm is probably due to the variability of the So-Rad R_{rs} (490) for some spectra in correspondence of HTSRB R_{rs} (490) values of 0.0050 sr^{-1} (Figure 10). The higher APD values in the red spectral region are likely due to the residuals of the glint/NIR corrections. These accuracy metrics are broadly comparable to the in-water/above-water comparison in (Pitarch et al., 2020) and are deemed good results considering that there was no control on measuring the same patch of water (HTSRB is ~50-100m from the vessel, So-Rad ~10m from the vessel). Moreover, as HTSRB was only deployed at stations with calm sea and clear sky conditions, these comparison statistics probably present a bias towards the best measuring conditions.

https://doi.org/10.5194/essd-2026-623
Preprint. Discussion started: 21 August 2026

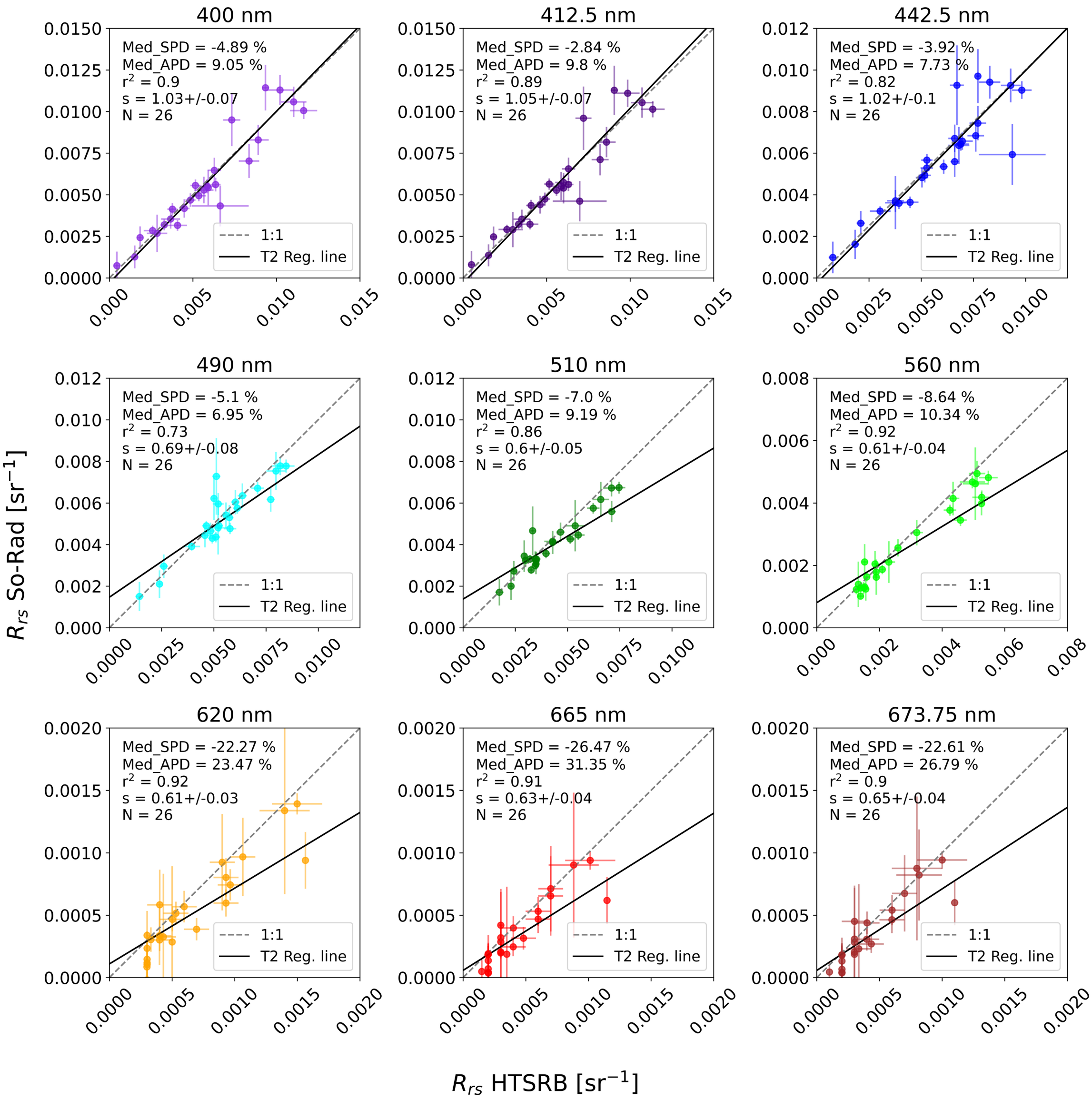

Figure 10 Example of optical closure exercise for radiometry. So-Rad (above-water) vs HTSRB (in-water) regression plots and accuracy metrics for different OLCI-S3 bands. So-Rad R_{rs} were BRDF-corrected to nadir viewing geometry for consistency with HTSRB. Match-up metrics (Med_SPD: median signed percentage difference, Med_APD: median absolute percentage difference, s: regression slope , r^2 : co-efficient of determination, are shown in each panel legend). *s* and *r* are both derived using Type 2 major-axis uncertainty weighting, and the 1-sigma propagated uncertainties for each system (as available in the full data files) are shown as cross-hairs in the scatter plots.

https://doi.org/10.5194/essd-2026-623
Preprint. Discussion started: 21 August 2026

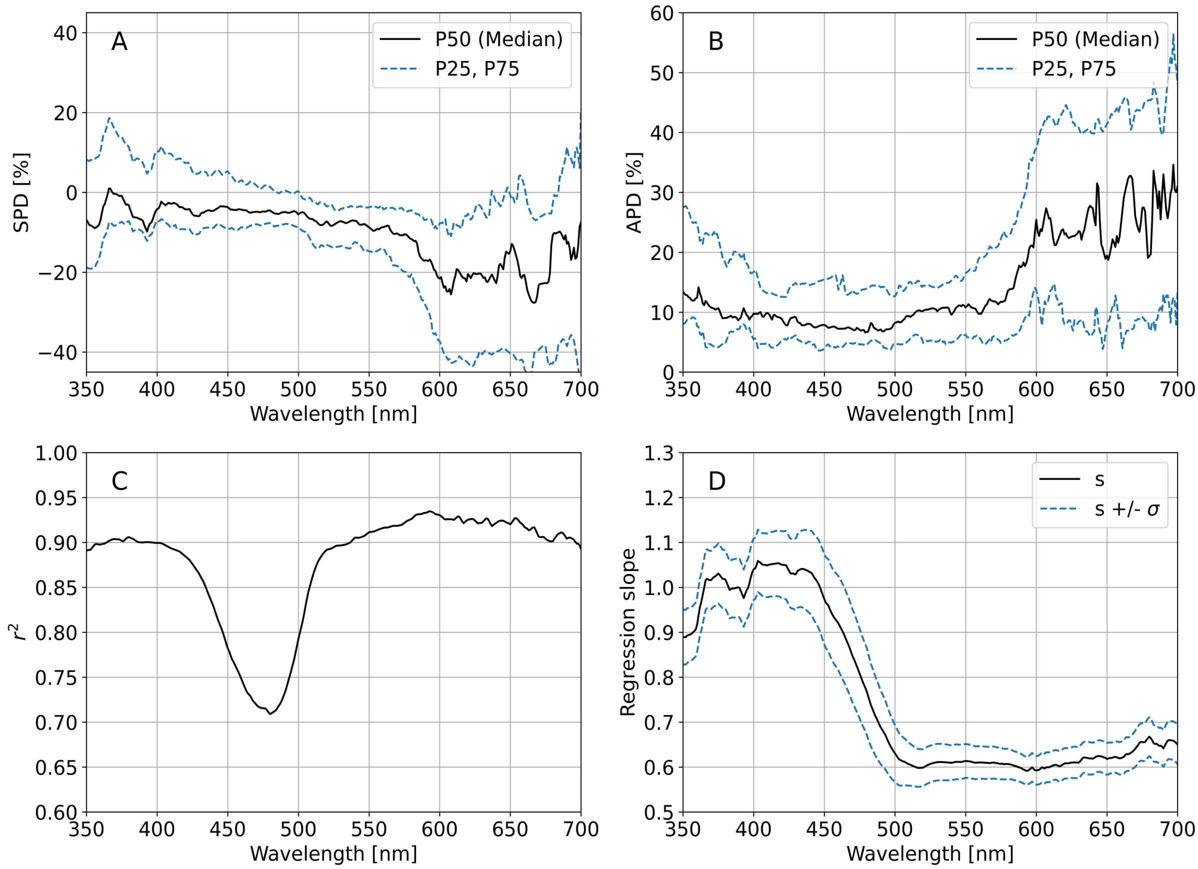

Figure 11 Spectral closure metrics for So-Rad vs HTSRB comparison: A. Median and quartiles for signed percentage difference (SPD) and. B. Absolute percentage difference (APD). C r^2. D. Regression slope (s) with 1-sigma uncertainty bounds

6 Data availability

All the original data and single variable files are available on the HyperBOOST project Zenodo page at https://doi.org/10.5281/ZENODO.15849296 as tabulated data and in SeaBASS format for the in-line IOPs, HTSRB and So-Rad spectra (Santinelli et al., 2026). The collocated dataset presented in this work is available at the Zenodo database (Costanzo et al., 2026b) at https://doi.org/10.5281/zenodo.18340674. The three files are available in full open access. Some of data presented in this work may be reprocessed if/when new data processing and quality assurance or control schemes become available. In these cases, a new version of the dataset will be created and uploaded on Zenodo.

https://doi.org/10.5194/essd-2026-623
Preprint. Discussion started: 21 August 2026

7 Summary and conclusions

The HyperBOOST hyperspectral dataset was acquired across the major European seas in 2023 and 2024 during 409 days of the expedition. Samples were collected at 202 stations, while along track data was collected for IOP and AOPS; after binning and quality control, 236,567 a_p and c_p spectra, 26,589 b_{bp} spectra and 7001 So-Rad R_{rs} spectra were available for further analyses and colocation with the station data. The HyperBOOST hyperspectral dataset covered and extended ranges previous reported for European waters for several bio-optical properties (e.g. Babin et al., 2003b, a; Nechad et al., 2015; Zibordi and Berthon, 2024) and for organic carbon measurements (Lønborg et al., 2024; Santinelli, 2015).

The data presented in this work was acquired consistently throughout the expedition: samples were collected following the same protocols and analysed with the same instrumentation in the same laboratories; hence they are comparable without the need of intercalibration. Furthermore, the excellent agreement among replicates supports the good quality of the data and the ability of Tara sampling teams.

The optical closure exercises presented in this work demonstrated the internal consistency of the IOPs and AOPs collected during the voyage, thus confirming that inline IOP measurements can provide high-quality data and showing that Tara is suitable platform to acquire continuous above-water was radiometry so long as robust quality control is applied.

The HyperBOOST dataset is relevant for the validation of current ocean colour satellite missions in optically complex waters (e.g. Gonzalez Vilas et al., 2026). Mass specific amplitude and the shape factors for IOPs that can be derived from this dataset will be analysed and presented in future work and will be the basis for future algorithm development refinement and for simulation for future hyperspectral missions (e.g. CHIME, S3-NGO). Furthermore, algorithms to derive new variables were developed using this dataset, as the apportioning of the inline a_p into a_{phy} and a_{NAP} (Costanzo et al., 2026a) and the estimate of the inline of a_{CDOM} from Seapoint FDOM fluorescence (Bourdin et al., 2026).

Integration of the HyperBOOST hyperspectral dataset with the imaging and -omics data collected during the Tara Europa Expedition will enable biodiversity and biological oceanography studies and the development of novel Earth observation product and datasets.

8 Team list

TREC-EMBL and Tara EUROPA Operation and Management Team: Paola Y. Bertucci, Peer Bork, Stefanie Kandels, Valerie Maier, Marta Major, Cristian Tambley, Kerstin Leberecht, Stephane Pesant, Matej Trojak, Colomban de Vargas, Douglas Couet, Morgane Guillam, Alienor Bourdrais, Alix Abautrais, Clementine Moulin

TREC Consortium Coordinators group: Samuel Abiven, Detlev Arendt, Hugo Berthelot, Paola Bertucci, Emmanuel Boss, Chris Bowler, Vittorio Brando, Colomban de Vargas, Johan Decelle, Gautam Dey, Michel Flores, Lionel Guidi, Niko Leisch, Fabien Lombard, Rainer Pepperkok, Georg

https://doi.org/10.5194/essd-2026-623
Preprint. Discussion started: 21 August 2026

Pohnert, Chiara Santinelli, Yannick Schwab, Raffaele Siano, Shinichi Sunagawa, Matthew Sullivan, Leho Tedersoo, Flora Vincent, Patrick Wincker, Sheree Yau, Michael Zimmermann

Tara Europa Team: Giancarlo Bachi, Odette Beluche, Hugo Berthelot, Paola Bertucci, Alienor Bourdais, Emmanuel Boss, Vittorio E. Brando, Juliette Cailliau, Solenne Caous, Ulisse Cardini, Samuel Chaffron, Douglas Couet, Iole Di Capua, Federico Falcini, Michel Flores, Jessika Fuessel, Morgane Guillam, Laure Guillou, Maïa Henry, Thomas Linkowski Fabien Lombard, Christian Marchese, Clémentine Moulin, James O'Brien, Léa Olivier, Gwenael Piganeau, Eric Pelletier, Julie Poulain, Chiara Santinelli, Shinichi Sunagawa, Flora Vincent, Patrick Wincker, Colomban de Vargas

9 Author contributions.

Conceptualization:VEB,FF, EB, DD CS, MHR, PB, CdV and VMV; Data curation: Mco,VEB, CM, LGV, EB, DD, PP, TJ, JW, CS and GB; Formal analysis: Mco, VEB, CM, LGV, EB, DD, PP, TJ, CS and VMV; Funding acquisition: VEB, EB, MHR, PB, CDV and VMV; Investigation (including field sampling and lab work): Mco, VEB, FF, CM, EB, DD, PP, TJ, CS, GB, GC, CT, Mca, MG, SV, VE and CdV; Methodology: Mco,VEB, FF, EB, DD, TJ, CS, GB, MHR, JAC, PB, CdV and VMV; Project administration: VEB, MHR, JAC, PB, CdV andVMV; Software: Mco, CM, LGV, SS and TJ; Supervision: VEB, CS, MHR, JAC andVMV; Validation: Mco, VEB, LGV, EB and TJ; Visualization: Mco, VEB, EB and TJ; Writing – original draft: Mco, VEB, CM, EB, DD, PP, TJ, CS and VMV; Writing – review & editing:Mco, VEB, CM, EB, DD, SS, TJ, CS, CdV and VMV.

10 Acknowledgements.

We thank the TREC consortium, the Tara Europa team, the TREC core partners of EMBL, the Tara Ocean Foundation, and the European Marine Biological Resource Centre (EMBRC) for their commitment to making the TREC-Tara Europa joint expedition possible. Special thanks to the the LSI Team, the AML Plankton Team, the SMS Team, the R/V Tara crew, and the many volunteers from partner research institutions across 21 European coastal countries who generously contributed their time and expertise to sampling efforts both at sea and on land.

We are grateful to the UK NERC Earth Observation Data Acquisition and Analysis Service (NEODAAS) for the loan of the So-Rad system in the HyperBOOST project. We also would like to thank the software team from HyperCP for their help in developing data processing methods for the So-Rad system.We also thank EUMETSAT and the Copernicus Marine Environment and Monitoring Service (CMEMS) for providing free ocean- color satellite data and the European Marine Observation and Data Network (EMODnet) for bathymetry data as these were used to support the sampling design. Thanks to the scientists and crew of the Tara Europa expedition for their efforts in the collection of quality inline data. Thanks to Tara technical crew and scientists on board for installation of the instrument and management of logistics, and Guillaume Bourdin for his contribution in processing the raw Tara Europa AC-S data. Thanks to A. Govind-shashikumar, I. Mayot, and to the SAPIGH service (https://lov.imev-mer.fr/web/facilities/sapigh/) for the extraction, HPLC analysis, and spectrophotometric measurements of Tara Europa pigment and samples.

We also sincerely thank the participating countries for graciously granting sampling permissions and acknowledge the institutional partners of the Tara Ocean Foundation—Fonds Français pour l'Environnement Mondial, UNESCO, Office Français de la Biodiversité (OFB), Région Bretagne, Lorient Agglomération, Lyon Métropole, and Terre Bleue Cotentin—for their trust and continued support.

Finally, we dedicate a special tribute to Peer Bork, whose vision initiated and profoundly shaped the Traversing European Coastlines (TREC) project. Peer passed away on January 16, 2026. His scientific leadership, unwavering commitment to collaborative and interdisciplinary research, and extraordinary intellectual contributions laid the foundations of this ambitious pan-European endeavour which opens the path toward a new era of planetary biology.

This paper is publication number (TBD) of the Traversing European Coastlines (TREC) Consortium.

11 **Financial support.**

The TREC and Tara Europa joint expedition was made possible through the generous financial support of: (i) the EMBL Member States through EMBL's Molecules to Ecosystems Programme (2022–2026); (ii) the European Union's Horizon Europe research and innovation programme through the BIOcean5D (Grant No. 101059915) and BlueRemediomics (Grant No. 101082304) projects; (iii) the European Space Agency (ESA) - funded Hyperspectral Bio-Optical Observations Sailing on Tara (HyperBOOST) project (grant number 4000135756/21/I-EF), and (iv) the generous support of the Tara Ocean Foundation from agnès b. and Etienne Bourgois, AXA, Bic, BNP Paribas, Capgemini, L'Oréal, Biotherm, the Veolia Foundation, Neuflize OBC, CNR, Bell & Ross, the EDF Foundation, the Rothschild Foundation, France Collectivités, and numerous individual donors. The collection and analysis of the inline IOP data and HyperPro was supported by NASA grant 80NSSC24K0374.

12 References

Aurin, D., Gossn, J. I., Bialek, A., Ramsey, A., Haëntjens, N., Costa, M., and Deru, A.: HyperInSPACE Community Processor (HyperCP) standardizes in situ above water radiometry processing including end-to-end uncertainties in compliance with protocols and Fiducial Reference Measurement standards, American Geophysical Union, Ocean Sciences Meeting, ADS Bibcode: 2024AGUOSOB53B..03A, OB53B-03, 2024.

Babin, M. and Stramski, D.: Variations in the mass-specific absorption coefficient of mineral particles suspended in water, Limnology & Oceanography, 49, 756–767, https://doi.org/10.4319/lo.2004.49.3.0756, 2004.

Babin, M., Morel, A., Fournier-Sicre, V., Fell, F., and Stramski, D.: Light scattering properties of marine particles in coastal and open ocean waters as related to the particle mass concentration, Limnology and Oceanography, 48, 843–859, https://doi.org/10.4319/lo.2003.48.2.0843, 2003a.

https://doi.org/10.5194/essd-2026-623
Preprint. Discussion started: 21 August 2026

Babin, M., Stramski, D., Ferrari, G. M., Claustre, H., Bricaud, A., Obolensky, G., and Hoepffner, N.: Variations in the light absorption coefficients of phytoplankton, nonalgal particles, and dissolved organic matter in coastal waters around Europe, Journal of Geophysical Research: Oceans, 108, https://doi.org/10.1029/2001JC000882, 2003b.

Blasco, T., Migon, C., Morin, G., Dufour, A., Vigier, N., Marty, S., and Doxaran, D.: Carbon stable isotope ratio as a revealer of incomplete decarbonation for particulate organic carbon measurement in river plumes, Geo-Mar Lett, 41, 4, https://doi.org/10.1007/s00367-020-00676-2, 2021.

Boss, E. and Pegau, W. S.: Relationship of light scattering at an angle in the backward direction to the backscattering coefficient, Appl. Opt., 40, 5503, https://doi.org/10.1364/AO.40.005503, 2001.

Boss, E., Picheral, M., Leeuw, T., Chase, A., Karsenti, E., Gorsky, G., Taylor, L., Slade, W., Ras, J., and Claustre, H.: The characteristics of particulate absorption, scattering and attenuation coefficients in the surface ocean; Contribution of the Tara Oceans expedition, Methods in Oceanography, 7, 52–62, https://doi.org/10.1016/j.mio.2013.11.002, 2013.

Boss, E., Haëntjens, N., Ackleson, S. G., Balch, B., Chase, A., Dall'Olmo, G., Freeman, S., Liu, Y., Loftin, J., Neary, W., Nelson, N., Novak, M., Slade, W. H., Proctor, C., Tortell, P., and Westberry, T. K.: Inherent Optical Property Measurements and Protocols: Best Practices for the Collection and Processing of Ship- Based Underway Flow-Through Optical Data (v4.0), IOCCG Protocol Series, 4, 17, https://doi.org/http://dx.doi.org/10.25607/OBP-458, 2019.

Bourdin, G., Gray, P., Doxaran, D., Sentinelli, C., Roesler, C., Chase, A., Haëntjens, N., and Boss, E.: Improved estimates of particulate absorption and attenuation with the Seabird's AC-S in flow-through mode using a CDOM fluorometer and a novel scattering correction., https://doi.org/10.1364/opticaopen.32587437, 10 June 2026.

Brando, V., Santoleri, R., Colella, S., Volpe, G., Di Cicco, A., Sammartino, M., González Vilas, L., Lapucci, C., Böhm, E., Zoffoli, M., Cesarini, C., Forneris, V., La Padula, F., Mangin, A., Jutard, Q., Bretagnon, M., Bryère, P., Demaria, J., Calton, B., Netting, J., Sathyendranath, S., D'Alimonte, D., Kajiyama, T., Van Der Zande, D., Vanhellemont, Q., Stelzer, K., Böttcher, M., and Lebreton, C.: Overview of Operational Global and Regional Ocean Colour Essential Ocean Variables Within the Copernicus Marine Service, Remote Sensing, 16, 4588, https://doi.org/10.3390/rs16234588, 2024.

Chase, A., Boss, E., Zaneveld, R., Bricaud, A., Claustre, H., Ras, J., Dall'Olmo, G., and Westberry, T. K.: Decomposition of in situ particulate absorption spectra, Methods in Oceanography, 7, 110–124, https://doi.org/10.1016/j.mio.2014.02.002, 2013.

Chase, A. P., Boss, E., Cetinić, I., and Slade, W.: Estimation of Phytoplankton Accessory Pigments From Hyperspectral Reflectance Spectra: Toward a Global Algorithm, JGR Oceans, 122, 9725–9743, https://doi.org/10.1002/2017JC012859, 2017.

https://doi.org/10.5194/essd-2026-623
Preprint. Discussion started: 21 August 2026

Costanzo, M., Brando, V. E., Boss, E., Chase, A., and Doxaran, D.: A novel approach to estimate non-algal particle absorption for improved retrieval of pigment concentrations in coastal waters, Limnology & Ocean Methods, e70073, https://doi.org/10.1002/lom3.70073, 2026a.

Costanzo, M., Brando, V., Marchese, C., Jordan, T., Santinelli, C., Doxaran, D., Boss, E., Simis, S., Potin, P., and Martinez Vicente, V.: Hyperspectral Bio-Optical Observations Sailing on Tara (HyperBOOST) Collocated In situ Dataset, https://doi.org/10.5281/ZENODO.18340674, 2026b.

Dall'Olmo, G., Westberry, T. K., Behrenfeld, M. J., Boss, E., and Slade, W. H.: Significant contribution of large particles to optical backscattering in the open ocean, Biogeosciences, 6, 947–967, https://doi.org/10.5194/bg-6-947-2009, 2009.

De Vargas, C., Audic, S., Henry, N., Decelle, J., Mahé, F., Logares, R., Lara, E., Berney, C., Le Bescot, N., Probert, I., Carmichael, M., Poulain, J., Romac, S., Colin, S., Aury, J.-M., Bittner, L., Chaffron, S., Dunthorn, M., Engelen, S., Flegontova, O., Guidi, L., Horák, A., Jaillon, O., Lima-Mendez, G., Lukeš, J., Malviya, S., Morard, R., Mulot, M., Scalco, E., Siano, R., Vincent, F., Zingone, A., Dimier, C., Picheral, M., Searson, S., Kandels-Lewis, S., Tara Oceans Coordinators, Acinas, S. G., Bork, P., Bowler, C., Gorsky, G., Grimsley, N., Hingamp, P., Iudicone, D., Not, F., Ogata, H., Pesant, S., Raes, J., Sieracki, M. E., Speich, S., Stemmann, L., Sunagawa, S., Weissenbach, J., Wincker, P., Karsenti, E., Boss, E., Follows, M., Karp-Boss, L., Krzic, U., Reynaud, E. G., Sardet, C., Sullivan, M. B., and Velayoudon, D.: Eukaryotic plankton diversity in the sunlit ocean, Science, 348, 1261605, https://doi.org/10.1126/science.1261605, 2015.

Dierssen, H., Bracher, A., Brando, V., Loisel, H., and Ruddick, K.: Data Needs for Hyperspectral Detection of Algal Diversity Across the Globe, Oceanog, 33, 74–79, https://doi.org/10.5670/oceanog.2020.111, 2020.

Dierssen, H. M., Vandermeulen, R. A., Barnes, B. B., Castagna, A., Knaeps, E., and Vanhellemont, Q.: QWIP: A Quantitative Metric for Quality Control of Aquatic Reflectance Spectral Shape Using the Apparent Visible Wavelength, Front. Remote Sens., 3, 869611, https://doi.org/10.3389/frsen.2022.869611, 2022.

Dogliotti, A. I., Ruddick, K. G., Nechad, B., Doxaran, D., and Knaeps, E.: A single algorithm to retrieve turbidity from remotely-sensed data in all coastal and estuarine waters, Remote Sensing of Environment, 156, 157–168, https://doi.org/10.1016/j.rse.2014.09.020, 2015.

Galletti, Y., Gonnelli, M., Retelletti Brogi, S., Vestri, S., and Santinelli, C.: DOM dynamics in open waters of the Mediterranean Sea: New insights from optical properties, Deep Sea Research Part I: Oceanographic Research Papers, 144, 95–114, https://doi.org/10.1016/j.dsr.2019.01.007, 2019.

Gonzalez Vilas, L., Jordan, T., and Brando, V.: HYperBOOST D4.2 Final Product Validation Report, Zenodo, https://doi.org/10.5281/ZENODO.20933781, 2026.

https://doi.org/10.5194/essd-2026-623
Preprint. Discussion started: 21 August 2026

Earth System Science Data Discussions

Haëntjens, N.: Inlinino, 2026.

Haëntjens, N. and Boss, E.: Inlinino: A Modular Software Data Logger for Oceanography, Oceanog, 33, 80–84, https://doi.org/10.5670/oceanog.2020.112, 2020.

Hansell, D. A.: Dissolved Organic Carbon Reference Material Program, Eos, Transactions American Geophysical Union, 86, 318–318, https://doi.org/10.1029/2005EO350003, 2005.

IOCCG: Ocean Optics and Biogeochemistry Protocols for Satellite Ocean Colour Sensor Validation, Volume 6.0: Particulate Organic Matter Sampling and Measurement Protocols: Consensus Towards Future Ocean Color Missions., https://doi.org/10.25607/OBP-1646, 2021.

Jordan, T. M., Simis, S. G. H., Grötsch, P. M. M., and Wood, J.: Incorporating a Hyperspectral Direct-Diffuse Pyranometer in an Above-Water Reflectance Algorithm, Remote Sensing, 14, 2491, https://doi.org/10.3390/rs14102491, 2022.

Jordan, T. M., Simis, S. G. H., Selmes, N., Sent, G., Ienna, F., and Martinez-Vicente, V.: Spatial structure of in situ reflectance in coastal and inland waters: implications for satellite validation, Front. Remote Sens., 4, 1249521, https://doi.org/10.3389/frsen.2023.1249521, 2023.

Lee, Z. P., Du, K., Voss, K. J., Zibordi, G., Lubac, B., Arnone, R., and Weidemann, A.: An inherent-optical-property-centered approach to correct the angular effects in water-leaving radiance, Appl. Opt., 50, 3155, https://doi.org/10.1364/AO.50.003155, 2011.

Lombard, F., Boss, E., Waite, A. M., Vogt, M., Uitz, J., Stemmann, L., Sosik, H. M., Schulz, J., Romagnan, J.-B., Picheral, M., Pearlman, J., Ohman, M. D., Niehoff, B., Möller, K. O., Miloslavich, P., Lara-Lpez, A., Kudela, R., Lopes, R. M., Kiko, R., Karp-Boss, L., Jaffe, J. S., Iversen, M. H., Irisson, J.-O., Fennel, K., Hauss, H., Guidi, L., Gorsky, G., Giering, S. L. C., Gaube, P., Gallager, S., Dubelaar, G., Cowen, R. K., Carlotti, F., Briseño-Avena, C., Berline, L., Benoit-Bird, K., Bax, N., Batten, S., Ayata, S. D., Artigas, L. F., and Appeltans, W.: Globally Consistent Quantitative Observations of Planktonic Ecosystems, Front. Mar. Sci., 6, 196, https://doi.org/10.3389/fmars.2019.00196, 2019.

Lønborg, C., Carreira, C., Abril, G., Agustí, S., Amaral, V., Andersson, A., Arístegui, J., Bhadury, P., Bif, M. B., Borges, A. V., Bouillon, S., Calleja, M. L., Cotovicz Jr., L. C., Cozzi, S., Doval, M., Duarte, C. M., Eyre, B., Fichot, C. G., García-Martín, E. E., Garzon-Garcia, A., Giani, M., Gonçalves-Araujo, R., Gruber, R., Hansell, D. A., Hashihama, F., He, D., Holding, J. M., Hunter, W. R., Ibánhez, J. S. P., Ibello, V., Jiang, S., Kim, G., Klun, K., Kowalczuk, P., Kubo, A., Lee, C.-W., Lopes, C. B., Maggioni, F., Magni, P., Marrase, C., Martin, P., McCallister, S. L., McCallum, R., Medeiros, P. M., Morán, X. A. G., Muller-Karger, F. E., Myers-Pigg, A., Norli, M., Oakes, J. M., Osterholz, H., Park, H., Lund Paulsen, M., Rosentreter, J. A., Ross, J. D., Rueda-Roa, D., Santinelli, C., Shen, Y., Teira, E., Tinta, T., Uher, G., Wakita, M., Ward, N., Watanabe, K., Xin, Y., Yamashita, Y., Yang, L., Yeo, J., Yuan, H., Zheng, Q., and Álvarez-Salgado, X. A.: A global database of dissolved organic matter (DOM)

https://doi.org/10.5194/essd-2026-623
Preprint. Discussion started: 21 August 2026

concentration measurements in coastal waters (CoastDOM v1), Earth System Science Data, 16, 1107–1119, https://doi.org/10.5194/essd-16-1107-2024, 2024.

Marchese, C., Boss, E., Falcini, F., Doxaran, D., and Vargas, C. de: Satellite Data Sharing for Scientific Inter-Group Cooperation Using the Leaflet R Package, Oceanography, 37, 70–74, https://doi.org/10.5670/oceanog.2024.513, 2024.

Massicotte, P., Babin, M., Fell, F., Fournier-Sicre, V., and Doxaran, D.: The Coastal Surveillance Through Observation of Ocean Color (COASTℓOOC) dataset, Earth System Science Data, 15, 3529–3545, https://doi.org/10.5194/essd-15-3529-2023, 2023.

Mobley, C. D.: Estimation of the remote-sensing reflectance from above-surface measurements, Appl. Opt., 38, 7442, https://doi.org/10.1364/AO.38.007442, 1999.

Morel, A. and Maritorena, S.: Bio-optical properties of oceanic waters: A reappraisal, J. Geophys. Res., 106, 7163–7180, https://doi.org/10.1029/2000JC000319, 2001.

Nechad, B., Ruddick, K., Schroeder, T., Oubelkheir, K., Blondeau-Patissier, D., Cherukuru, N., Brando, V., Dekker, A., Clementson, L., Banks, A. C., Maritorena, S., Werdell, P. J., Sá, C., Brotas, V., Caballero De Frutos, I., Ahn, Y.-H., Salama, S., Tilstone, G., Martinez-Vicente, V., Foley, D., McKibben, M., Nahorniak, J., Peterson, T., Siliò-Calzada, A., Röttgers, R., Lee, Z., Peters, M., and Brockmann, C.: CoastColour Round Robin data sets: a database to evaluate the performance of algorithms for the retrieval of water quality parameters in coastal waters, Earth Syst. Sci. Data, 7, 319–348, https://doi.org/10.5194/essd-7-319-2015, 2015.

Neukermans, G., Loisel, H., Mériaux, X., Astoreca, R., and McKee, D.: In situ variability of mass-specific beam attenuation and backscattering of marine particles with respect to particle size, density, and composition, Limnology & Oceanography, 57, 124–144, https://doi.org/10.4319/lo.2012.57.1.0124, 2012.

Pitarch, J., Talone, M., Zibordi, G., and Groetsch, P.: Determination of the remote-sensing reflectance from above-water measurements with the "3C model": a further assessment, Opt. Express, 28, 15885, https://doi.org/10.1364/OE.388683, 2020.

Ras, J., Claustre, H., and Uitz, J.: Spatial variability of phytoplankton pigment distributions in the Subtropical South Pacific Ocean: comparison between in situ and predicted data, Biogeosciences, 5, 353–369, https://doi.org/10.5194/bg-5-353-2008, 2008.

Röttgers, R., McKee, D., and Woźniak, S. B.: Evaluation of scatter corrections for ac-9 absorption measurements in coastal waters, Methods in Oceanography, 7, 21–39, https://doi.org/10.1016/j.mio.2013.11.001, 2013.

https://doi.org/10.5194/essd-2026-623
Preprint. Discussion started: 21 August 2026

Ruddick, K. G., De Cauwer, V., Park, Y.-J., and Moore, G.: Seaborne measurements of near infrared water-leaving reflectance: The similarity spectrum for turbid waters, Limnol. Oceanogr., 51, 1167–1179, https://doi.org/10.4319/lo.2006.51.2.1167, 2006.

Santinelli, C.: DOC in the Mediterranean Sea, in: Biogeochemistry of Marine Dissolved Organic Matter, Elsevier, 579–608, https://doi.org/10.1016/B978-0-12-405940-5.00013-3, 2015.

Santinelli, C., Follett, C., Retelletti Brogi, S., Xu, L., and Repeta, D.: Carbon isotope measurements reveal unexpected cycling of dissolved organic matter in the deep Mediterranean Sea, Marine Chemistry, 177, 267–277, https://doi.org/10.1016/j.marchem.2015.06.018, 2015.

Santinelli, C., Jordan, T., Doxaran, D., Boss, E., Marchese, C., Simis, S., Meek, E., Brando, V., Wood, J., Potin, P., and Martinez-Vicente, V.: Hyperboost In-situ data (v6 added discrete pabs, TSM, POC), https://doi.org/10.5281/ZENODO.15849296, 2026.

Slade, W. H., Boss, E., Dall'Olmo, G., Langner, M. R., Loftin, J., Behrenfeld, M. J., Roesler, C., and Westberry, T. K.: Underway and Moored Methods for Improving Accuracy in Measurement of Spectral Particulate Absorption and Attenuation, Journal of Atmospheric and Oceanic Technology, 27, 1733–1746, https://doi.org/10.1175/2010JTECHO755.1, 2010.

Sullivan, J. M., Twardowski, M. S., Zaneveld, J. R. V., Moore, C. M., Barnard, A. H., Donaghay, P. L., and Rhoades, B.: Hyperspectral temperature and salt dependencies of absorption by water and heavy water in the 400-750 nm spectral range, Appl. Opt., 45, 5294, https://doi.org/10.1364/AO.45.005294, 2006.

Sullivan, J. M., Twardowski, M. S., Ronald, J., Zaneveld, V., and Moore, C. C.: Measuring optical backscattering in water, in: Light Scattering Reviews 7, Springer Berlin Heidelberg, Berlin, Heidelberg, 189–224, https://doi.org/10.1007/978-3-642-21907-8_6, 2013.

Sunagawa, S., Coelho, L. P., Chaffron, S., Kultima, J. R., Labadie, K., Salazar, G., Djahanschiri, B., Zeller, G., Mende, D. R., Alberti, A., Cornejo-Castillo, F. M., Costea, P. I., Cruaud, C., d'Ovidio, F., Engelen, S., Ferrera, I., Gasol, J. M., Guidi, L., Hildebrand, F., Kokoszka, F., Lepoivre, C., Lima-Mendez, G., Poulain, J., Poulos, B. T., Royo-Llonch, M., Sarmento, H., Vieira-Silva, S., Dimier, C., Picheral, M., Searson, S., Kandels-Lewis, S., Tara Oceans coordinators, Bowler, C., De Vargas, C., Gorsky, G., Grimsley, N., Hingamp, P., Iudicone, D., Jaillon, O., Not, F., Ogata, H., Pesant, S., Speich, S., Stemmann, L., Sullivan, M. B., Weissenbach, J., Wincker, P., Karsenti, E., Raes, J., Acinas, S. G., Bork, P., Boss, E., Bowler, C., Follows, M., Karp-Boss, L., Krzic, U., Reynaud, E. G., Sardet, C., Sieracki, M., and Velayoudon, D.: Structure and function of the global ocean microbiome, Science, 348, 1261359, https://doi.org/10.1126/science.1261359, 2015.

Sunagawa, S., Acinas, S. G., Bork, P., Bowler, C., Tara Oceans Coordinators, Acinas, S. G., Babin, M., Bork, P., Boss, E., Bowler, C., Cochrane, G., De Vargas, C., Follows, M., Gorsky, G., Grimsley, N., Guidi, L., Hingamp, P., Iudicone, D., Jaillon, O., Kandels, S., Karp-Boss, L., Karsenti, E., Lescot, M.,

https://doi.org/10.5194/essd-2026-623
Preprint. Discussion started: 21 August 2026

Not, F., Ogata, H., Pesant, S., Poulton, N., Raes, J., Sardet, C., Sieracki, M., Speich, S., Stemmann, L., Sullivan, M. B., Sunagawa, S., Wincker, P., Eveillard, D., Gorsky, G., Guidi, L., Iudicone, D., Karsenti, E., Lombard, F., Ogata, H., Pesant, S., Sullivan, M. B., Wincker, P., and De Vargas, C.: Tara Oceans: towards global ocean ecosystems biology, Nat Rev Microbiol, 18, 428–445, https://doi.org/10.1038/s41579-020-0364-5, 2020.

Tilstone, G. H., Jordan, T. M., Aurin, D., Białek, A., Deru, A., Ramsay, A., Hieronymi, M., Dall'Olmo, G., Ligi, M., Kovach, C., Ansko, I., Ondrusek, M., Vabson, V., Zibordi, G., Gossn, J. I., Kwiatkowska, E., and Vendt, R.: Radiometric field inter-comparison of fiducial reference measurements using an open source community processor, Opt. Express, 33, 15756, https://doi.org/10.1364/OE.551042, 2025.

Vabson, V., Ansko, I., Bialek, A., Feinholz, M. E., Kuusk, J., Lamb, R., Marty, S., Ondrusek, M., Rammeloo, C., Rehm, E., Vendt, R., Voss, K. J., Gossn, J. I., and Kwiatkowska, E.: Laboratory Calibration Comparison of Hyperspectral Ocean Color Radiometers in the Frame of the FRM4SOC Phase 2 Project, Remote Sensing, 17, 3692, https://doi.org/10.3390/rs17223692, 2025.

Vandermeulen, R. A., Mannino, A., Craig, S. E., and Werdell, P. J.: 150 shades of green: Using the full spectrum of remote sensing reflectance to elucidate color shifts in the ocean, Remote Sensing of Environment, 247, 111900, https://doi.org/10.1016/j.rse.2020.111900, 2020.

Werdell, P. J., Proctor, C. W., Boss, E., Leeuw, T., and Ouhssain, M.: Underway sampling of marine inherent optical properties on the Tara Oceans expedition as a novel resource for ocean color satellite data product validation, Methods in Oceanography, 7, 40–51, https://doi.org/10.1016/j.mio.2013.09.001, 2013a.

Werdell, P. J., Proctor, C. W., Boss, E., Leeuw, T., and Ouhssain, M.: Underway sampling of marine inherent optical properties on the Tara Oceans expedition as a novel resource for ocean color satellite data product validation, Methods in Oceanography, 7, 40–51, https://doi.org/10.1016/j.mio.2013.09.001, 2013b.

Wood, J., Smyth, T. J., and Estellés, V.: Autonomous marine hyperspectral radiometers for determining solar irradiances and aerosol optical properties, Atmos. Meas. Tech., 10, 1723–1737, https://doi.org/10.5194/amt-10-1723-2017, 2017.

Wright, A. and Simis, S.: Construction of the Solar-tracking Radiometry platform (So-Rad), https://doi.org/10.5281/ZENODO.4485805, 2021.

Zaneveld, J. R. V., Kitchen, J. C., and Moore, C. C.: Scattering error correction of reflecting-tube absorption meters, Ocean Optics XII, 44–55, https://doi.org/10.1117/12.190095, 1994.

Zhang, X., Hu, L., and He, M.-X.: Scattering by pure seawater: Effect of salinity, Opt. Express, 17, 5698, https://doi.org/10.1364/OE.17.005698, 2009.

https://doi.org/10.5194/essd-2026-623
Preprint. Discussion started: 21 August 2026

Zhang, X., Hu, L., Gray, D., and Xiong, Y.: Shape of particle backscattering in the North Pacific Ocean: the χ factor, Appl. Opt., 60, 1260, https://doi.org/10.1364/AO.414695, 2021.

Zhou, L., Simon, K., Fradette, M., Leeuw, T., Xiong, Y., Huot, Y., and Zhang, X.: Angular weighting function of Hyper-bb instrument, Appl. Opt., 65, 7066, https://doi.org/10.1364/AO.603919, 2026.

Zibordi, G. and Berthon, J.-F.: Coastal Atmosphere and Sea Time Series (CoASTS) and Bio-Optical mapping of Marine Properties (BiOMaP): the CoASTS-BiOMaP dataset, Earth System Science Data, 16, 5477–5502, https://doi.org/10.5194/essd-16-5477-2024, 2024.